# Tamoxifen metabolites acting *via* $BK_{Ca}$ orchestrate the dynamics of $K^+$ and $Ca^{2+}$ in breast cancer cells

Received for publication, January 26, 2025, and in revised form, November 13, 2025 Published, Papers in Press, December 6, 2025
https://doi.org/10.1016/j.jbc.2025.111015

**Selina Maier[1,2], Werner Schroth[2], Finn Mier[3], Lucas Matt[1], Helmut Bischof[1], Aiden Tamaddon[1], Darko Stojkov[1], Lena Birkenfeld[1], Melanie Cruz Santos[1], Dominic Gross[1], Johanna Dahlen[1], Florian A. Büttner[2], Irina Bonzheim[4], Falko Fend[4], Hiltrud Brauch[2,5,6], Frank M. Boeckler[3,7], Matthias Schwab[2,5,6,8], and Robert Lukowski[1,*]**

*From the [1]Department of Pharmacology, Toxicology and Clinical Pharmacy, Institute of Pharmacy, University of Tübingen, Tübingen, Germany; [2]Dr. Margarete Fischer-Bosch Institute of Clinical Pharmacology, Stuttgart, Germany; [3]Laboratory for Molecular Design and Pharmaceutical Biophysics, Institute of Pharmacy, University of Tübingen, Tübingen, Germany; [4]Institute of Pathology and Neuropathology, University Hospital Tübingen, Tübingen, Germany; [5]Cluster of Excellence iFIT (EXC 2180) "Image-guided and Functionally Instructed Tumor Therapies", University of Tübingen, Tübingen, Germany; [6]German Cancer Consortium (DKTK) and German Cancer Research Center, Partner Site Tübingen, Tübingen, Germany; [7]Interfaculty Institute for Biomedical Informatics (IBMI), University of Tübingen, Tübingen, Germany; and [8]Departments of Clinical Pharmacology, and Biochemistry and Pharmacy, University of Tübingen, Tübingen, Germany*

Reviewed by members of the JBC Editorial Board. Edited by Mike Shipston

**The voltage- and calcium ($Ca^{2+}$)-activated potassium ($K^+$) channel of large conductance ($BK_{Ca}$) is aberrantly expressed in various breast cancer (BC) subtypes, including estrogen receptor (ER)-positive tumors. Increased proliferation of BC cells in response to tamoxifen (TAM) and its metabolites (TAM+M) has been shown to rely on the cell's $BK_{Ca}$ status. However, the mechanism by which TAM+M impact on $BK_{Ca}$ activity to promote malignancy is yet not clear. By examining murine MMTV-PyMT tumor-derived BC cells and human BC cell lines with a genetically encoded $K^+$ ion indicator and electrophysiological recordings, we identified $BK_{Ca}$-dependent intracellular $K^+$ signals and currents provoked by treatment with clinically relevant TAM+M in an ER-independent manner. In line with this, genetical or pharmacological blockade of $BK_{Ca}$ significantly diminished the TAM+M-induced modulation of $BK_{Ca}$ $K^+$ currents and consequently also the drop of intracellular $K^+$ ions in BC cells. Changes in the $K^+$ balance subsequently triggered intra- and extracellular $Ca^{2+}$ mobilization, which was in turn stimulated by the TAM+M-$BK_{Ca}$ axis. Our results highlight that $BK_{Ca}$ "oncochannels" may modulate the response of BC cells to TAM+M. Activation of the TAM+M-$BK_{Ca}$ axis causes significant changes in $K^+$ and $Ca^{2+}$ ion homeostasis, which ultimately contributes to the outcome of endocrine-based BC pharmacotherapy.**

Breast cancer (BC) is the most frequently diagnosed cancer and the leading cause of cancer-related death among women (1). BC comprises different subgroups based on the expression of the human epidermal growth factor receptor ($HER2^+$), the progesterone receptor ($PR^+$) and/or the estrogen receptor ($ER^+$) or triple-negative BC (TNBC) (2). Classical treatment often includes surgery, radiotherapy and, depending on the type of tumor, cytotoxic as well as endocrine therapy (3). In pursue of novel prognosticators, predictors, and putative treatment targets, molecular expression profiles defined four intrinsic BC subtypes (*i.e.* LumA, LumB, HER2-enriched, basal) (4), and more recently, a single-cell spatially resolved atlas revealed nine BC "ecotypes" (5). These recent insights into cell-based expression profiles enable better selection of therapeutic strategies and will promote target identification for novel personalized therapeutic approaches.

Ion channels have sparked interest as putative novel anticancer drug targets as they are frequently dysregulated in most cancer entities (6, 7). Of particular interest are potassium ($K^+$) channels that contribute to malignant cell proliferation by perturbating the membrane potential, cell volume and calcium ($Ca^{2+}$) signaling although $K^+$ channels can also influence cell migration, invasion and apoptosis (8).

The voltage- and $Ca^{2+}$-activated $K^+$ channel of large conductance (9) alias $BK_{Ca}$ or Slo1, is a transmembrane protein consisting of a tetramer of pore-forming α-subunits located in the plasma membrane (PM), Golgi apparatus, endoplasmic reticulum and mitochondria of BC cells (7, 10). Each α-subunit contains a voltage-sensing domain (S4) and two pore-forming loop segments (S5-S6) that cross the membrane. The cytoplasmic C-terminal tail of each α-subunit is composed of two high-affinity $Ca^{2+}$-sensing sites located in the regulator of conductance (RCK)1 and RCK2 domains (10). In BC, $BK_{Ca}$ promoted cell proliferation (7, 9, 11), metastatic spread, invasive growth in the brain (12) and was associated with high tumor stage and poor prognosis (11), hence, $BK_{Ca}$ has been termed an "oncochannel" (13). Other hormone-sensitive cancers, such as cervical (14) and prostate cancer

* For correspondence: Robert Lukowski, robert.lukowski@uni-tuebingen.de.
Present address for Helmut Bischof: Gottfried Schatz Research Center, Molecular Biology and Biochemistry, and Division of Oncology, Department of Internal Medicine, Medical University of Graz, Austria.

(15), and tumors that grow independently of hormones, such as glioma (16) and pancreatic ductal carcinoma (17), display altered $BK_{Ca}$ channel expression together with a higher potential of malignancy. Interestingly, 17β-Estradiol (E2) enhances the proliferation of $BK_{Ca}$-proficient murine and human BC cells (9), and particularly stimulates $BK_{Ca}$ channel activity in human MCF-7 BC cells (18). Independent evidence for a link between E2 and an increase of the $BK_{Ca}$ channel's open probability ($P_O$) was obtained from non-cancerous *Xenopus laevis* oocytes and smooth muscle cells in which these effects were mediated by the regulatory β1 subunit that increases the sensitivity of the channel complex to $Ca^{2+}$ (19–22).

In patients with BC having ER-positive tumors endocrine treatment with tamoxifen (TAM), high $BK_{Ca}$ α-subunit expression levels modified their outcome in an unfavorable manner. This was recapitulated in *in vitro* experiments with TAM and its metabolites (TAM+M) that stimulated the growth of human and murine BC cell lines in a $BK_{Ca}$-dependent manner (9) as well as $BK_{Ca}$'s $P_O$ in human MCF-7 cells (23). Both effects, *i.e.* a TAM-mediated increase in $BK_{Ca}$ activity and the modulation of $P_O$, have also been observed in other model systems such as murine and canine colonic myocytes, and they were again dependent on the presence of the $BK_{Ca}$ α and β1 subunits (24, 25). Similarly, the $P_O$ of avian $BK_{Ca}$ α-and β-subunit complexes can be modulated by TAM (26).

Mechanistically, hyperpolarization of the PM induced by $K^+$ channels such as $BK_{Ca}$ increases the driving force for $Ca^{2+}$ influx, for example, by store-operated $Ca^{2+}$ entry (SOCE) or constitutive $Ca^{2+}$ entry (CCE) (8). The resulting $Ca^{2+}$ signaling in BC cells has been fundamentally linked to processes underlying proliferation, invasion, metastasis and apoptosis (27) and can be potentiated with TAM as shown in MCF-7 cells exposed to agonists such ATP (28). The effect to release $Ca^{2+}$ from intracellular stores such as the endoplasmic reticulum as well as the TAM-modulated $Ca^{2+}$ entry through PM channels is likely ER-independent as it has been commonly observed in non-ER positive tumor cells such as human glioma (28), oral cancer cells (29), non-melanoma skin cancer (30), HepG2 human hepatoblastoma cells and bladder cancer cells (31), but also under physiological conditions in intact Madin-Darby canine kidney (MDCK) cells and human neutrophils (32) and platelets (33).

It remains, however, unclear whether and to what extent the effects of TAM on tumor-promoting $BK_{Ca}$ channel activity and on $Ca^{2+}$ signaling events depend on the same pathway in BC although such interactions between $BK_{Ca}$ and the cytosolic $Ca^{2+}$ are known from other cell systems (34–37).

Here, we investigated the impact of TAM+M on $BK_{Ca}$ channel activity and $Ca^{2+}$ signaling in murine and human BC cells using an integrated approach that on the one hand combined pharmacological tools and gene knockout models and on the other hand electrophysiological and imaging-based approaches for the visualization of $Ca^{2+}$ and $K^+$ ions in living cells with molecular docking strategies. These studies aimed to uncover the underlying molecular mechanisms by which the TAM+M-$BK_{Ca}$ axis contributes to the $Ca^{2+}$ homeostasis of BC cells and thus to malignant cell behaviors that promote cancer progression.

## Results

### $BK_{Ca}$ is expressed in clinically relevant BC biopsies and functionally relevant in human BC cells

Bulk gene expression analysis of 551 human derived BC specimen revealed different $K^+$ channel transcript levels in $ER^+$ BC. Consistent with a previous report (7), *KCNMA1* mRNA was significantly higher expressed in these BC specimens compared to other cancer-associated $K^+$ channels (*KCNA3*, *KCNH1*, *KCNH2*, *KCNK5*, *KCNK9*, *KCNN3*, and *KCNN4*). Interestingly, *KCNMA1*-derived transcripts were also present in all individual samples analyzed (Fig. 1*A*). Transcript levels of *KCNMA1* in the $ER^+$ human BC cell lines MCF-7 ($hBK_{Ca}^{low}$) and CAMA-1 ($hBK_{Ca}^{medium}$) and the $ER^-$ human BC cell line MDA-MB-453 ($hBK_{Ca}^{high}$) confirmed highest expression level of $BK_{Ca}$ channels in $hBK_{Ca}^{high}$ BC cells (Fig. 1*B*). An investigation of $BK_{Ca}$ channel subunits confirmed β-, γ-, and Lingo1 transcripts in the BC cell lines, which, however, showed significantly lower expression levels in $hBK_{Ca}^{high}$ compared to the pore-forming α-subunit of $BK_{Ca}$ (Fig. S1*A*).

To verify the functionality of $BK_{Ca}$ channels in these human BC cell lines, whole-cell patch-clamp recordings were performed to obtain current density-voltage relationships in $hBK_{Ca}^{low}$, $hBK_{Ca}^{medium}$ and $hBK_{Ca}^{high}$ BC cells. At +120 mV and physiological intracellular $Ca^{2+}$ concentrations ($[Ca^{2+}]_i$), $K^+$ outward currents of $hBK_{Ca}^{high}$ BC cells were significantly increased over $hBK_{Ca}^{medium}$ and $hBK_{Ca}^{low}$ BC cells (Fig. 1*C*). Representative current-over-time traces of $hBK_{Ca}^{low}$, $hBK_{Ca}^{medium}$ and $hBK_{Ca}^{high}$ (Fig. 1, *D–I* left) were normalized to cell size in current density calculations (Fig. 1, *D–I* right). $K^+$ outward currents that were reliably detected in response to depolarization steps in $hBK_{Ca}^{low}$ cells were insensitive to the specific $BK_{Ca}$ blocker paxilline (PAX) (Fig. 1*D*). In contrast, peak $K^+$ outward currents were significantly inhibited by PAX treatment in $hBK_{Ca}^{medium}$ and $hBK_{Ca}^{high}$ cells (Fig. 1, *E* and *F*), verifying previously reported patch-clamp recordings on $hBK_{Ca}$ localized in the PM of MCF-7 and MDA-MB-453 cells (7, 9).

Additionally, immunofluorescence (IF) staining shows a higher abundance of $BK_{Ca}$ in $hBK_{Ca}^{high}$ compared to $hBK_{Ca}^{low}$ BC cells (Fig. S1*B*), confirming whole-cell patch-clamp experiments. Importantly, phalloidin staining indicates that the cell size of $hBK_{Ca}^{low}$ and $hBK_{Ca}^{high}$ BC cells varies (Fig. S1*B*), explaining the differences in the conductance and the resulting current densities over time in the whole-cell patch-clamp recordings.

To further evaluate whether $hBK_{Ca}^{high}$ activity is sensitive to the $BK_{Ca}$ specific activator NS11021, the compound was added to the bath solution (Fig. 1*G*), resulting in higher $K^+$ outward currents during patch-clamp recordings. Further, we

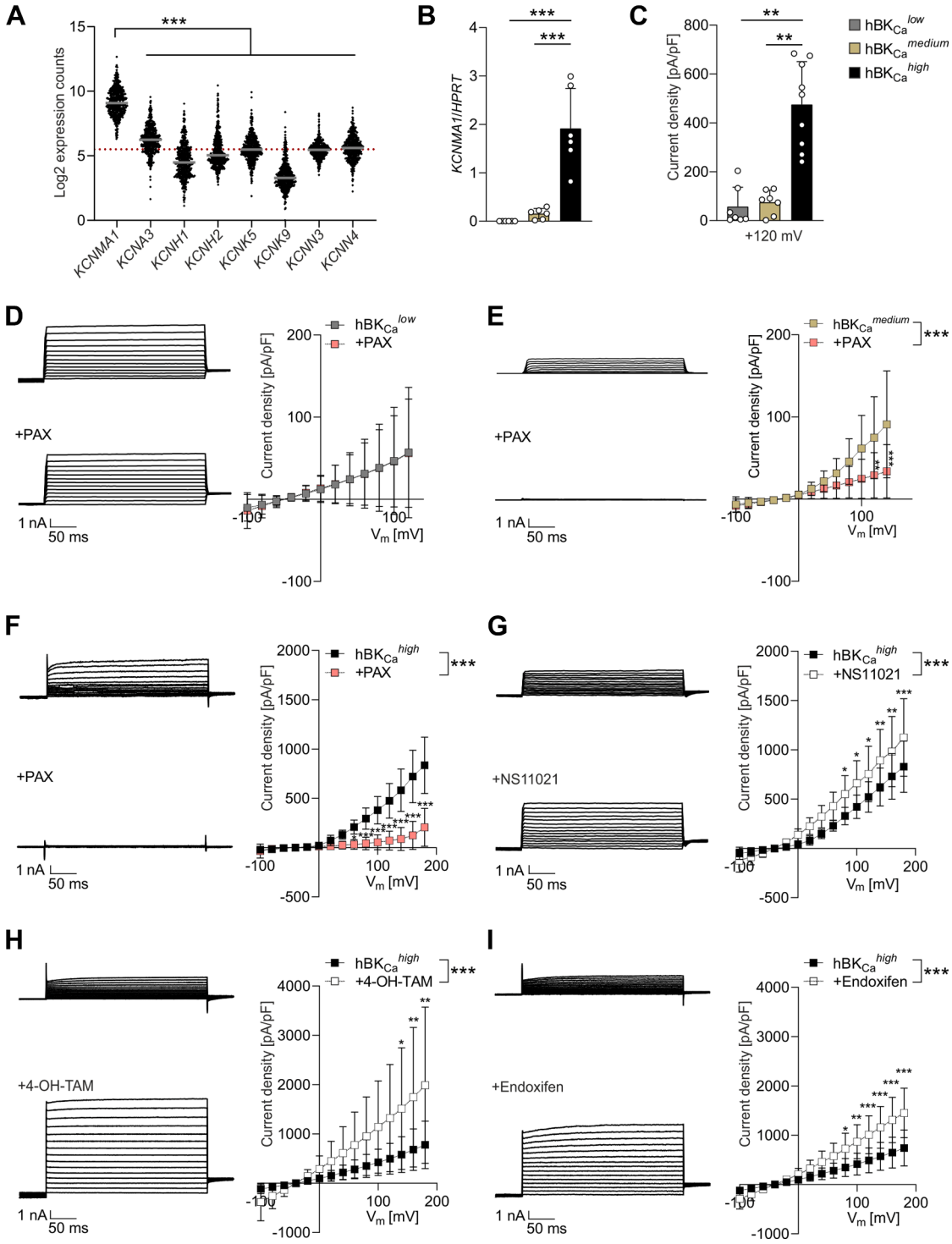


**Figure 1. BK$_{Ca}$ expression in human BC biopsies and electrophysio-/pharmacological properties of human BC cell BK$_{Ca}$ channels**. mRNA expression levels of (*A*) *KCNMA1* and selected cancer-associated $K^+$ channels from human BC biopsies (partly adapted from (7)) and (*B*) *KCNMA1* in human BC cell lines hBK$_{Ca}^{low}$, hBK$_{Ca}^{medium}$ and hBK$_{Ca}^{high}$. *C*, current-density-voltage relationships of hBK$_{Ca}^{low}$, hBK$_{Ca}^{medium}$ and hBK$_{Ca}^{high}$ compared at +120 mV (data of selected voltage was adapted from the recordings in *D–F*). *D–I*, representative whole-cell current recordings (*left*) and current density-voltage relationships (*right*) of hBK$_{Ca}^{low}$, hBK$_{Ca}^{medium}$ and hBK$_{Ca}^{high}$ BC cells, (*D*, *E*, *F*) before and during paxilline (PAX), (*G*) NS11021, (*H*) 4-OH-TAM, and (*I*) endoxifen treatment. Data represents average ± SD. n(biopsies) = (*A*) 551; n(independent experiments) = (*B*) 6; n(cells) = (*C*) 7-9, (*D*) 7, (*E*) 7, (*F*) 9, (*G*) 11, (*H*) 8, (*I*) 8, with *$p \leq 0.05$, **$p \leq 0.01$, ***$p \leq 0.001$. *A and C*, Kruskal-Wallis test followed by Dunn's multiple comparisons test. *B*, one-way ANOVA followed by Tukey's multiple comparisons test. *D–I* two-way ANOVA followed by Šídák's multiple comparisons test. Statistical values, probe and primer sequences are described in detail in Table S1, Table S10, and Table S11, respectively.

observed that TAM+M (4-OH-TAM and endoxifen) elevated $K^+$ outward currents in $hBK_{Ca}^{high}$ cells massively, and even more than NS11021 (Fig. 1, *H* and *I*), suggesting that TAM+M impacts the ion homeostasis of BC cells by modulating the subcellular $K^+$ homeostasis *via* $BK_{Ca}$ channel activation. Importantly, we observed that the majority of successfully measured $hBK_{Ca}^{high}$ cells indeed responded to 4-OH-TAM (72.73%) and endoxifen (61.54%) with increased $K^+$ currents (Fig. S1*C*), which is in line with the variability of $BK_{Ca}$ protein levels in individual $hBK_{Ca}^{high}$ cells (Fig. S1*B*). Potential reasons for this "patchy" $BK_{Ca}$ expression profile were not investigated, but might be explained by the previously demonstrated cell cycle-dependent variation of $K^+$ channel expression in non-cancerous and cancer cells (6, 38, 39), as our IF and patch-clamp experiments were carried out in non-synchronized cells.

Together, these findings confirm the presence of $BK_{Ca}$ channels in $ER^+$ human BC tissue and $hBK_{Ca}^{low/medium/high}$ BC cells. In addition, functional $BK_{Ca}$ channel expression in $hBK_{Ca}^{high}$ correlated with TAM+M-mediated effects on $K^+$ outward currents.

### TAM+M modulate $K^+$ dynamics through $BK_{Ca}$ independently of ER

Based on the observed effects on whole-cell currents by TAM+M (Fig. 1), we investigated $K^+$ homeostasis utilizing lc-LysM GEPII1.0, a well-established cytosolic FRET-based $K^+$ sensor (7, 40). Next to $hBK_{Ca}^{low}$, $hBK_{Ca}^{medium}$ and $hBK_{Ca}^{high}$ BC cell models, we additionally studied SKBr-3 ($ER^-$) as $hBK_{Ca}^{low}$ cell line (Fig. 2). The latter was selected based on the RNAseq data in Cancer Cell Line Encyclopedia (CCLE) library and included in our analysis to address how the absence of ER (and low $BK_{Ca}$) in human BC cells affect the response to TAM+M.

Alterations in cytosolic $K^+$ concentration ($[K^+]_i$) were first induced by the $BK_{Ca}$ channel opener NS11021 in MCF-7 $hBK_{Ca}^{low}$ ($ER^+$), CAMA-1 $hBK_{Ca}^{medium}$ ($ER^+$) and MDA-MB-453 $hBK_{Ca}^{high}$ ($ER^-$) (Fig. 2, *A* and *B*). $BK_{Ca}$ abundance of these cells correlated with the $[K^+]_i$ loss, which was significantly different in $hBK_{Ca}^{high}$ ($ER^-$) compared to the $[K^+]_i$ response seen in $hBK_{Ca}^{medium}$ ($ER^+$) and $hBK_{Ca}^{low}$ ($ER^+$), strongly suggesting that these $[K^+]_i$ alterations occurred irrespective of the ER status of the cells (Fig. 2*B*). Importantly, in $hBK_{Ca}^{low}$ cells expressing RFP-tagged $BK_{Ca}$ (+$BK_{Ca}$-$RFP^{rescue}$) we consistently observed a massive drop in $[K^+]_i$ compared to respective control $hBK_{Ca}^{low}$ ($ER^+$) cells, regardless of whether RFP (+RFP) was present or not (Fig. 2*A*). In addition, we made use of a previously mapped panel of patient-derived $BK_{Ca}$ loss- and gain-of-function mutations (41). Interestingly, one of the loss-of-function channel variants carries the G354S mutation (41), a site residing within the selectivity filter of $BK_{Ca,}$ which is highly conserved among $K^+$ selective ion channels (42). This loss-of-function mutant results in a "pore-death" variant of $BK_{Ca}$ with dramatically reduced $K^+$ conductance and a lower selectivity to $K^+$, which causes symptoms like ataxia, dyskinesias and cognitive impairment in a young patient carrying the $BK_{Ca}$ G354S mutation (43). We induced the G354S mutation in our established $BK_{Ca}$-RFP construct by site-directed mutagenesis. Importantly, the expression of $BK_{Ca}^{G354S}$-RFP (+$BK_{Ca}^{G354S}$) in $hBK_{Ca}^{low}$ ($ER^+$) BC cells demonstrated levels comparable to the empty vector control (+RFP) and "wild type" $BK_{Ca}$-$RFP^{rescue}$ (Fig. S1*D*). FRET-based $K^+$ recordings evoked by NS11021 in $hBK_{Ca}^{low}$ ($ER^+$) BC cells expressing $BK_{Ca}^{G354S}$ were, however, significantly impaired compared to functional "wild type" $BK_{Ca}$-$RFP^{rescue}$ channels (Fig. 2*A*). Employing a related $BK_{Ca}$ channel opener, NS1619, showed similar effects on $[K^+]_i$ in $hBK_{Ca}^{low}$ ($ER^+$) and $hBK_{Ca}^{high}$ ($ER^-$) BC cells (Fig. S1*E*).

To test if 4-OH-TAM and endoxifen impact the cell's $K^+$ dynamics in a $BK_{Ca}$- and/or concentration-dependent manner, we analyzed $[K^+]_i$ in $hBK_{Ca}^{low}$ ($ER^+$) and $hBK_{Ca}^{high}$ ($ER^-$) cell lines. Indeed, 4-OH-TAM induced a significantly higher drop of $[K^+]_i$ in $hBK_{Ca}^{high}$ ($ER^-$) compared to $hBK_{Ca}^{low}$ ($ER^+$) cells, an effect that was consistent for all concentrations tested (Figs. 2*C* and S1*F*). Furthermore, administration of endoxifen resulted in a concentration-dependent $K^+$ loss in $hBK_{Ca}^{high}$ ($ER^-$) as indicated by the decreasing FRET ratio signal. At the maximal concentration tested, differences in $[K^+]_i$ in $hBK_{Ca}^{low}$ ($ER^+$) and $hBK_{Ca}^{high}$ ($ER^-$) reached the level of significance (Fig. 2*D*). In addition, we compared the FRET ratio signals recorded from SKBR-3 $hBK_{Ca}^{low}$ ($ER^-$) and $hBK_{Ca}^{medium}$ ($ER^+$) to $hBK_{Ca}^{low}$ ($ER^+$) and $hBK_{Ca}^{high}$ ($ER^-$) BC cells treated with endoxifen. This analysis validated that the TAM+M-mediated $K^+$ loss correlated with the $BK_{Ca}$ expression level but occurred irrespective of the cell's ER status (Figs. 2*E* and S1*G*). Subsequently, we excluded the potential interference caused by growth factors and steroid hormones. Therefore, cells were cultured in charcoal-stripped bovine serum (CCS), a reagent leading to significant hormone deprivation, before monitoring live-cell $K^+$ changes by FRET imaging. In $hBK_{Ca}^{low}$ and $hBK_{Ca}^{high}$ BC cells, we reproduced previous findings on TAM+M-induced $[K^+]_i$ alterations, suggesting that the response to TAM+M is independent of media supplements, *i.e.* of endocrine pathways (Fig. S2, *A* and *B*).

To more directly evaluate whether steroid hormones influence the $K^+$ homeostasis in a manner comparable to the anti-estrogenic TAM+M, we investigated changes in the $K^+$ FRET ratio signal in response to E2. Pro-proliferative effects of E2 on human BC cells and stimulatory effects on $BK_{Ca}$ channels have been reported (9, 18) but strikingly, at least in non-cancerous tissue, may exclusively depend on $BK_{Ca}$'s auxiliary subunit β1 (21, 22). In the observed timeframe, however, live-cell $K^+$ imaging revealed only minor effects of E2 on the $K^+$ balance in $hBK_{Ca}^{low}$ and $hBK_{Ca}^{high}$, and no differences between both BC cell models, suggesting E2 is linked to $BK_{Ca}$ by a different mode of action (Fig. 2*F*).

To additionally validate and broaden our data on TAM+M-mediated $[K^+]_i$, endoxifen was administered to $hBK_{Ca}^{low}$-expressing $BK_{Ca}$-$RFP^{rescue}$ or loss-of-function mutant $BK_{Ca}^{G354S}$ cells or cells solely expressing RFP as a control. Compared to $hBK_{Ca}^{low}$, $BK_{Ca}$-$RFP^{rescue}$ expressing BC cells showed a massive decrease of $[K^+]_i$, whereas cells expressing

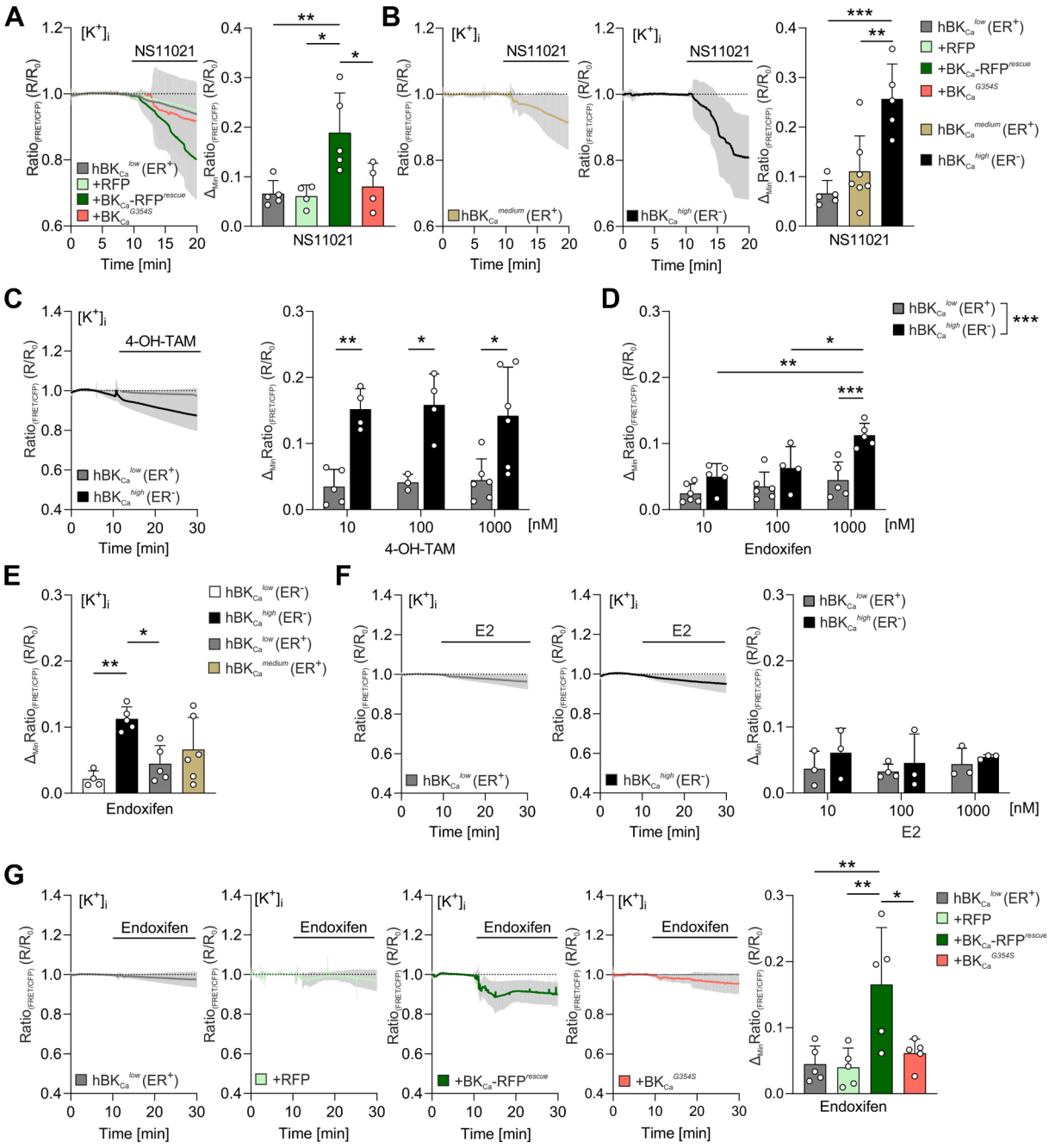


**Figure 2. TAM+M trigger cytosolic K$^+$ dynamics in BC cells independently of ER.** (*A*, *B*, *C*, *F*, *and G*), K$^+$ FRET-ratio signals obtained by live-cell imaging of cytosolic K$^+$ concentrations ([K$^+$]$_i$) over time of hBK$_{Ca}^{low}$ (ER$^+$ or ER$^-$), hBK$_{Ca}^{medium}$ (ER$^+$) and hBK$_{Ca}^{high}$ (ER$^-$) BC cells and (*A–G*) corresponding bar charts with individual data points for statistical analysis, which is based on the difference of the basal (R$_0$) to the minimal (R) K$^+$ FRET/CFP ratio signals and expressed as $\Delta_{Min}$(R/R$_0$). Alterations of [K$^+$]$_i$ were induced by bath-administration of (*A*, *B*) BK$_{Ca}$ activator NS11021 (hBK$_{Ca}^{low}$ from *A* adapted in *B*), active TAM metabolites (*C*) 4-OH-TAM and (*D*, *E*, *G*) endoxifen or (*F*) E2 following 10 min of FRET recording at basal conditions. ER$^+$ hBK$_{Ca}^{low}$ cells expressed in addition either (*A*, *G*) RFP (+RFP), RFP-tagged BK$_{Ca}$ (+BK$_{Ca}$-RFP$^{rescue}$) or RFP-tagged "pore-death" BK$_{Ca}^{G354S}$ (+BK$_{Ca}^{G354S}$) as indicated. FRET-ratio signal responses are displayed for (*C*, *E*, *G*) 1 μM 4-OH-TAM or endoxifen and (*F*) 1 μM E2. Data represents average ± SD. n(independent experiments) = (*A*) 4-5, (*B*) 5-7, (*C*) 3-6, (*D*) 4-6, (*E*) 4-6, (*F*) 3-4, (*G*) 5 with *$p \le 0.05$, **$p \le 0.01$, ***$p \le 0.001$. (*A*, *B*, *E*, *G*) One-way ANOVA followed by Tukey's multiple comparisons test and (*C*, *D*, *F*) Two-way ANOVA followed by Tukey's multiple comparisons test with significant group differences in (*C*, *D*). Statistical values are described in detail in Table S2.

only RFP did not exhibit a drop in [K$^+$]$_i$, *i.e.* FRET signals remained at the level of hBK$_{Ca}^{low}$ (Fig. 2*G* and S2*C*). "Pore-death" BK$_{Ca}^{G354S}$ expression in hBK$_{Ca}^{low}$ prevented the endoxifen-induced [K$^+$]$_i$ loss compared to BK$_{Ca}$-RFP$^{rescue}$ channels (Fig. 2*G*), supporting the hypothesis of a TAM+M-promoted BK$_{Ca}$ activity.

Finally, loss of [K$^+$]$_i$ should lead to an increased extracellular K$^+$ concentration ([K$^+$]$_{ex}$). To examine [K$^+$]$_{ex}$, we applied recombinant purified GEPII1.0 as previously described (40, 44). Gramicidin, a K$^+$ ionophore, was used to induce maximal K$^+$ release from cells (Fig. S2*D*). Also, we observed a clear trend for 4-OH-TAM and a significant increase of [K$^+$]$_{ex}$

in $hBK_{Ca}^{high}$ BC cells treated with endoxifen (Fig. S2*E*), confirming that the decrease in $[K^+]_i$ ultimately results in an efflux of $K^+$ to the extracellular space.

In sum, TAM+M treatment initiates a cascade causing a drop of $[K^+]_i$ and consequently elevated $[K^+]_{ex}$ levels. The $K^+$ alterations observed are closely related to the cell's $BK_{Ca}$ channel abundance but occur independently of the ER status of all BC cell lines studied.

### TAM+M-mediated effects on $K^+$ dynamics are abolished by genetic or pharmacological inactivation of endogenous $BK_{Ca}$ channels

In a BC mouse model based on the mouse mammary tumor virus (MMTV) polyoma middle T antigen (PyMT), genetic ablation of the $BK_{Ca}$ α-subunit showed beneficial outcomes regarding tumor-free and overall survival in comparison to respective $BK_{Ca}$-proficient control littermates. Interestingly, and contrary to expectations from clinical use of the anti-estrogenic compounds, TAM+M treatment promoted the proliferative behavior of isolated murine BC cells obtained from the MMTV-PyMT model only in the presence of $BK_{Ca}$ (9). Based on these previous studies, murine MMTV-$PyMT^{tg/+}$ WT ($mBK_{Ca}^{WT}$) and BKKO ($mBK_{Ca}^{KO}$) derived BC cells were isolated from primary tumors and the cytosol-targeted $K^+$ sensor lc-LysM GEPII1.0 was expressed to study basal $[K^+]_i$ and changes induced by TAM+M. In agreement with the live-cell imaging experiments in human BC cells, endoxifen and 4-OH-TAM induced a $BK_{Ca}$-dependent drop in $[K^+]_i$ (Fig. 3, *A* and *B* and Fig. S2*F*). Further, $K^+$ efflux in $mBK_{Ca}^{WT}$ was sensitive to PAX, resulting in $[K^+]_i$ loss equalizing with the one observed in $mBK_{Ca}^{KO}$ (Fig. 3*A*). Accordingly, TAM+M-induced $BK_{Ca}$-mediated $[K^+]_i$ changes in $hBK_{Ca}^{high}$ ($ER^-$) (hereafter referred to as $hBK_{Ca}^{high}$) were sensitive to PAX, whereas $hBK_{Ca}^{low}$ ($ER^+$) (hereafter referred to as $hBK_{Ca}^{low}$) did not respond to pharmacological $BK_{Ca}$ channel inhibition (Fig. 3, *C* and *D* and Fig. S2*G*).

These findings support the notion that murine and human $BK_{Ca}$ channels respond similarly to TAM+M with respect to the effect of these compounds on the cell's $K^+$ balance. Further, genetic and pharmacological inhibition of endogenous $BK_{Ca}$ prevented the observed alterations in $[K^+]_i$ pointing towards a common TAM+M–$BK_{Ca}$ axis.

### TAM+M stimulate a rise in $[Ca^{2+}]_i$ levels through $BK_{Ca}$

Multiple hallmarks of cancer are influenced by alterations in $K^+$ channels expression and $Ca^{2+}$ ion dynamics including cell cycle control, migration and adhesion, as well as apoptosis (45, 46). Previous work indicated that cancer cell $Ca^{2+}$ signaling is affected by aberrant $K^+$ channel expression (47). Mechanistically, $K^+$ channel activation and the resulting $K^+$ efflux provide a driving force for $Ca^{2+}$ influx (8, 48). Therefore, we examined the potential influence of TAM+M on

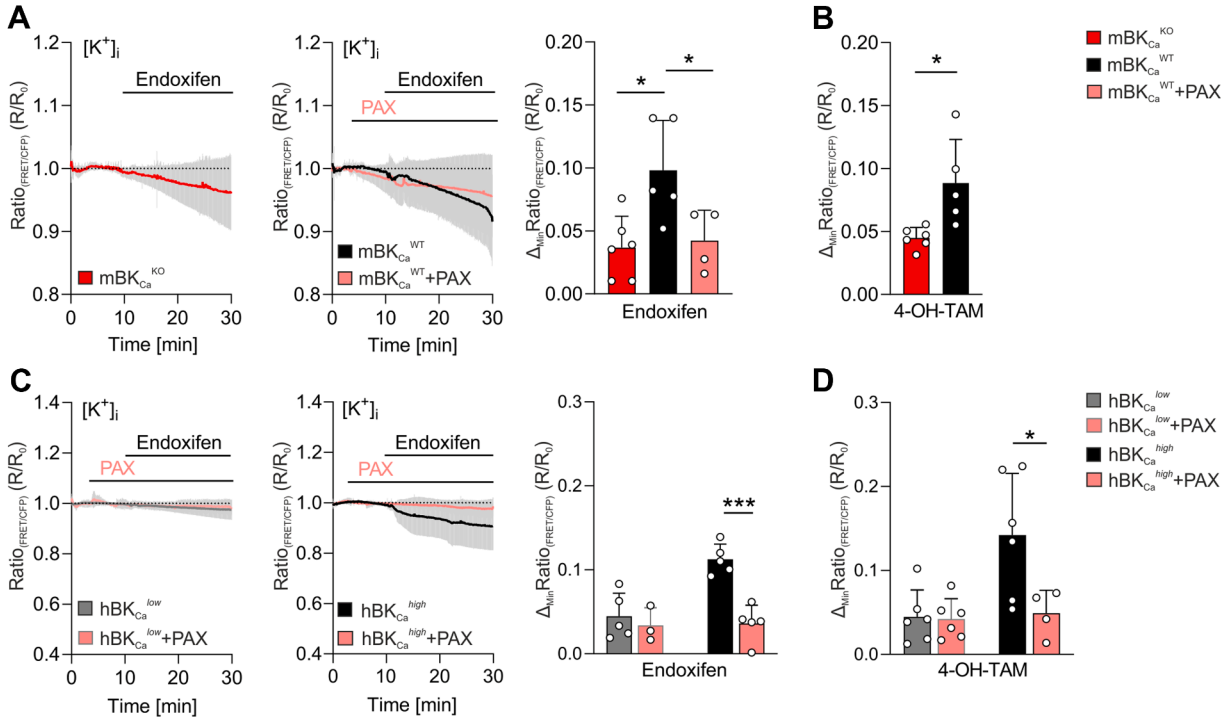


**Figure 3. TAM+M-mediated effects on murine and human BC cell $K^+$ homeostasis require functional $BK_{Ca}$ channels.** *A–D*, FRET-ratio signals and corresponding statistics of cytosolic $K^+$ ($[K^+]_i$) dynamics over time in murine MMTV-PyMT $BK_{Ca}$ WT ($mBK_{Ca}^{WT}$) and KO ($mBK_{Ca}^{KO}$) and human $hBK_{Ca}^{low}$ and $hBK_{Ca}^{high}$ BC cells. Live-cell $K^+$ imaging was performed prior and after bath-application of (*A*) endoxifen, (*B*) 4-OH-TAM, (*A* and *C*) PAX+endoxifen and (*D*) PAX+4-OH-TAM. *C*, PAX+endoxifen and (*D*) PAX+4-OH-TAM treated $hBK_{Ca}^{low}$ and $hBK_{Ca}^{high}$ BC cells were compared with 1 μM 4-OH-TAM and 1 μM endoxifen (Fig. 2, *C* and *D*) respectively. Data represents average ± SD. n(isolated tumors) = (*A* and *B*) 4-6 and n(independent experiments) = (*C*) 3-5, (*D*) 4-6 with $*p \le 0.05$ and $***p \le 0.001$. *A*, one-way ANOVA followed by Tukey's multiple comparisons test. (*B*) Unpaired *t* test. *C* and *D* two-way ANOVA followed by Šídák's multiple comparisons test. Statistics are described in detail in Table S3.

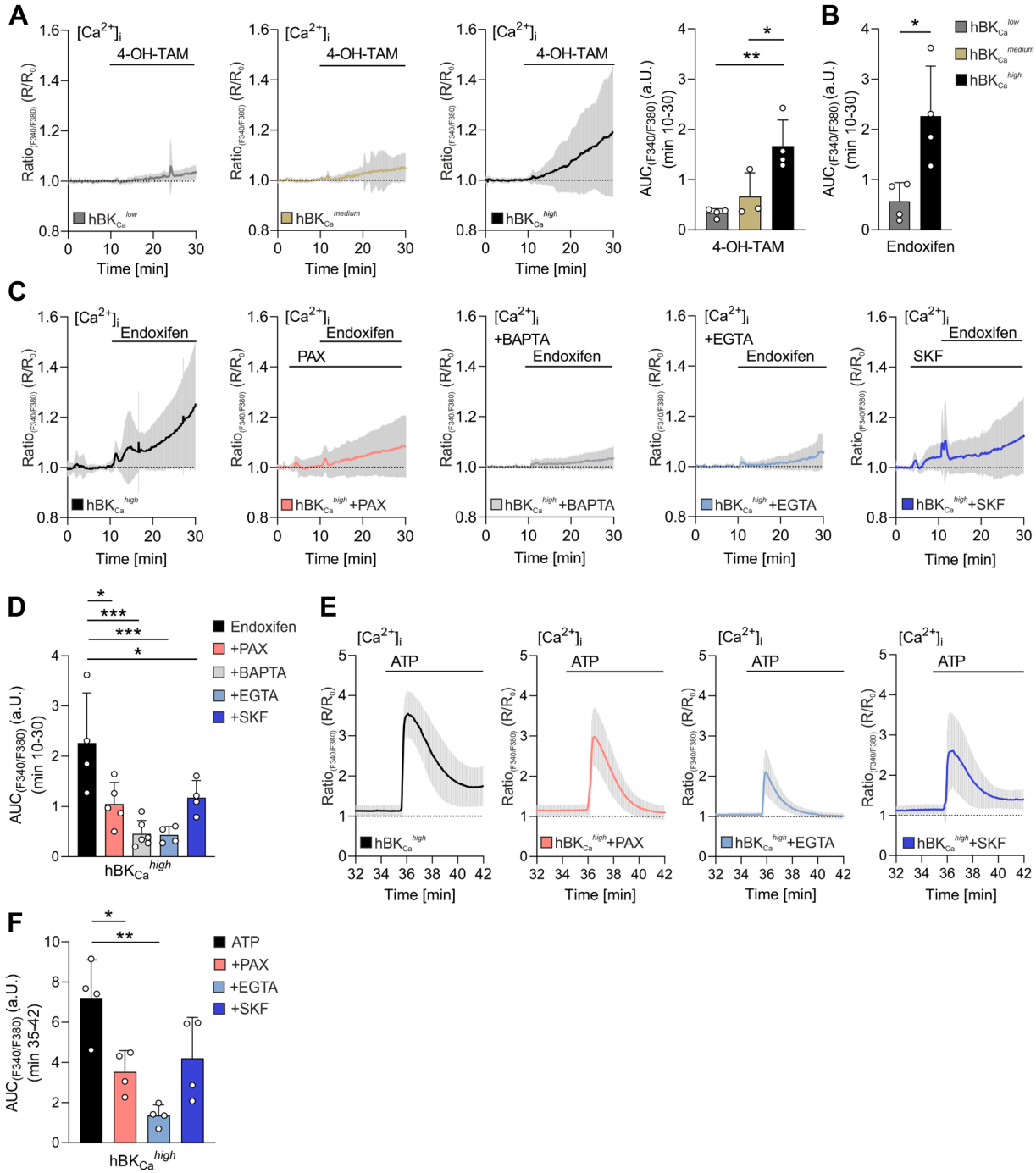


**Figure 4. TAM+M-induced $BK_{Ca}$ activation elevates $[Ca^{2+}]_i$.** Fluorescence emission ratio signals over time and area under the curve (AUC) statistics of $hBK_{Ca}^{low}$, $hBK_{Ca}^{medium}$, and $hBK_{Ca}^{high}$ BC cells loaded with the ratiometric $Ca^{2+}$ dye Fura-2 in presence of (*A*) 4-OH-TAM or (*B*) endoxifen. Fluorescence emission ratio traces ($F_{340}/F_{380}$) of $hBK_{Ca}^{low}$ (Fig. S3*A*) were compared with $hBK_{Ca}^{high}$ (Fig. 4*C*). $F_{340}/F_{380}$ nm emission ratio for Fura-2 loaded (*C*) $hBK_{Ca}^{high}$ BC cells in response to endoxifen in addition with further treatment by (from *left* to *right*) $BK_{Ca}$ inhibitor PAX, BAPTA AM (BAPTA) for intracellular $Ca^{2+}$ depletion, EGTA-buffered extracellular $Ca^{2+}$-free solution, and TRP/C, STIM/ORAI1 channel blocker SKF-96365 (SKF). *D*, analysis of the area under the curve (AUC) of Fura-2 loaded $hBK_{Ca}^{high}$ BC cells under recording conditions specified in (*C*). *E*, fura-2 fluorescence emission ratio signals ($F_{340}/F_{380}$ nm) in response to $Ca^{2+}$ changes over time and statistics obtained from monitoring $hBK_{Ca}^{high}$ BC cells after pre-treatment with endoxifen, PAX+endoxifen, EGTA+endoxifen, SKF+endoxifen (from *left* to *right*) followed by extracellular ATP application to provoke emptying of intracellular $Ca^{2+}$ stores. *F*, analysis of the AUC of Fura-2 loaded $hBK_{Ca}^{high}$ BC cells under recording conditions specified in (*E*) *i.e.* after endoxifen pre-treatment (for 20 min followed by a 5 min washout) in addition to the treatments as specified in the panels. Data represents average ± SD. n(independent experiments) = (*A*, *B*) 3-4, (*C*, *D*) 4-6, (*E*, *F*) 4, with $*p \le 0.05$, $**p \le 0.01$, $***p \le 0.001$. *A*, *D*, *F*, one-way ANOVA followed by Tukey's multiple comparisons test. *B*, unpaired *t* test. Statistical values are described in detail in Table S4.

$Ca^{2+}$ homeostasis using Fura-2, a ratiometric ($F_{340}/F_{380}$) $Ca^{2+}$ indicator. 4-OH-TAM administration elevated $[Ca^{2+}]_i$ levels in a $BK_{Ca}$-dependent manner. Accordingly, the rise in Fura-2 ratio was significantly lower in $hBK_{Ca}^{low}$ and $hBK_{Ca}^{medium}$ cells compared to $hBK_{Ca}^{high}$ cells (Fig. 4*A*). Application of the alternative TAM+M endoxifen confirmed these results as the largest increase in $[Ca^{2+}]_i$ was induced in $hBK_{Ca}^{high}$ (Fig. 4*B*). We also treated $hBK_{Ca}^{low}$ ($ER^-$) cells with endoxifen and observed a similar increase in the $Ca^{2+}$ signal compared to $hBK_{Ca}^{low}$ ($ER^+$) cells (Fig. S3*A*), indicating TAM+M act on $Ca^{2+}$, independent from ER-mediated genomic events.

Next, we monitored $[Ca^{2+}]_i$ in $hBK_{Ca}^{high}$ cells exposed to endoxifen and PAX for pharmacological $BK_{Ca}$ inhibition. Under these co-treatment conditions, the endoxifen-induced increase in Fura-2 ratio was significantly diminished, suggesting that TAM+M require functional $BK_{Ca}$ channels to affect $[Ca^{2+}]_i$ (Fig. 4, *C* and *D*). To examine the $Ca^{2+}$ accumulation in response to TAM+M in more detail, we depleted intra- and extracellular $Ca^{2+}$ stores by administration of BAPTA AM (BAPTA) and EGTA, a cell-permeant and -impermeant chelator of $Ca^{2+}$, respectively, in $Ca^{2+}$-free buffer. Under both conditions Fura-2 ratio signals were significantly decreased during TAM+M treatment (Fig. 4, *C* and *D*), suggesting that $Ca^{2+}$ mobilization across the PM from extracellular sources and from intracellular stores contributes to the observed increase in $[Ca^{2+}]_i$. In BC cells, $Ca^{2+}$ release from the endoplasmic reticulum is recognized by the $Ca^{2+}$ store sensor protein STIM and results in SOCE, which is an important mechanism to raise $[Ca^{2+}]_i$. Ultimately, SOCE is triggering a $Ca^{2+}$ entry pathway involving PM $Ca^{2+}$ channels (f. ex. ORAI) to restore $[Ca^{2+}]_i$ (49). High log2 transcript expression counts of *STIM1*, *ORAI1* and *ORAI3* were identified by gene expression analysis of human BC biopsies (Fig. S3*B*). In subsequent Fura-2 experiments, we used SKF-96365 (SKF), an inhibitor of SOCE (50) and TRP/C channels (51). We recognized an initial increase in $[Ca^{2+}]_i$ levels (Fig. 4*C*) which was also previously observed to be induced in nasopharyngeal carcinoma cells by SKF-mediated release of $Ca^{2+}$ in the endoplasmic reticulum (52) or, by directly affecting $Ca^{2+}$ entry in human leukemic HL-60 and MDCK cells (53, 54) and/or by enhancing $Na^+/Ca^{2+}$ exchanger function in glioblastoma cells (55). After Fura-2 fluorescence emission ratio signals stabilized in response to SKF, endoxifen treatment was still effective in increasing $[Ca^{2+}]_i$, albeit not to the same extent as in the absence of SKF (Fig. 4, *C* and *D*). We conclude from the Fura-2 measurements that STIM-ORAI complexes, as well as PM $Ca^{2+}$ channels (TRP/C), contribute to the $BK_{Ca}$-dependent cellular $[K^+]_i$ loss in response to endoxifen.

To investigate the influence of TAM+M on the mobilization of $Ca^{2+}$ from intracellular stores, $hBK_{Ca}^{high}$ were stimulated with adenosin-5′-triphosphate (ATP) that acts through purinergic receptors to subsequently trigger the release of $Ca^{2+}$ from endoplasmic reticulum *via* inositol-triphosphate ($IP_3$) (56–58). ATP was applied following pre-treatment of the cells with endoxifen under basal conditions or in the presence of PAX, EGTA or SKF (Fig. 4*E* from left to right). Statistical analyses revealed significantly lower levels of ATP-induced release of $Ca^{2+}$ to accumulate as $[Ca^{2+}]_i$ under PAX and EGTA conditions (Fig. 4*F*). These results indicate TAM+M-induced $BK_{Ca}$-dependent $K^+$ dynamics increase the driving force for $Ca^{2+}$ uptake from both extracellular and intracellular stores. Because PAX-mediated inhibition of $BK_{Ca}$ decreased the ATP-induced rise in $[Ca^{2+}]_i$, we conclude that $Ca^{2+}$ released from intracellular stores is functionally linked to $Ca^{2+}$-activated $BK_{Ca}$ channel activity and thus part of a feed-forward mechanism.

Using Fura-2 as $Ca^{2+}$ sensitive probe highlights that TAM+M, through $BK_{Ca}$ activation, causes a $K^+$ loss across the PM, which enhances the driving force for $Ca^{2+}$ influx *via* PM localized store- and non-store- operated $Ca^{2+}$ channels. It additionally appears that $Ca^{2+}$ release from intracellular stores, *i.e.* the endoplasmic reticulum, contributes to the observed rise in $[Ca^{2+}]_i$. $hBK_{Ca}^{low}$ BC cells or pharmacological channel blockade reduced all TAM+M-induced changes in $[Ca^{2+}]_i$, proving that $BK_{Ca}$ activity is essential to functionally connect TAM+M to $Ca^{2+}$ signaling.

### TAM+M-induced $BK_{Ca}$-activity mediates voltage-and $Ca^{2+}$ alterations which sustain $BK_{Ca}$ stimulation

As TAM+M affects $BK_{Ca}$-dependent $K^+$ and $Ca^{2+}$ dynamics, we next monitored $[K^+]_i$, again employing the FRET-based $K^+$ probe lc-LysM GEPII1.0 while (i) chelating intracellular $Ca^{2+}$ using BAPTA AM, (ii) under $Ca^{2+}$-free conditions with extracellular EGTA, and after blockade of PM TRP/C and STIM/ORAI using SKF. Interestingly, none of these experimental conditions prevented induction of the TAM+M-mediated drop in $[K^+]_i$ (Fig. 5*A*). Importantly, the initial drop in $[K^+]_i$ induced by SKF did not lead to continuous $BK_{Ca}$ activation in absence of endoxifen (Fig. S3*C*).

Hence, the systematic elimination of intra- and extracellular $Ca^{2+}$ sources did not interfere with the TAM+M-induced $BK_{Ca}$-dependent $K^+$ dynamics in $hBK_{Ca}^{high}$, indicating that the interaction of TAM+M with $BK_{Ca}$ precedes any subsequent events on $[Ca^{2+}]_i$ (Fig. 5*B*). To confirm these $K^+$ live-cell imaging results, whole-cell patch-clamp experiments were performed under EGTA-buffered, $Ca^{2+}$-free conditions to record current density-voltage relationships of $hBK_{Ca}^{high}$ cells. In the absence of $[Ca^{2+}]_{ex}$, we again identified significantly elevated $K^+$ outward currents in response to endoxifen (Fig. 5*C*), while the patch success rate decreased under EGTA-buffered conditions (Figs. S1*C*, 50%) compared to physiological $[Ca^{2+}]_{ex}$-buffered bath solution (Fig. 1*I* and S1*C*, 61.54%).

The observed changes in ion homeostasis and in particular the activation of $BK_{Ca}$ should affect the membrane potential of BC cells. The fluorescent and slow-response voltage-sensitive probe $DiBAC_4(3)$ (59) was therefore used to detect changes in $\Psi_{PM}$ ($\Delta\Psi_{PM}$) in $hBK_{Ca}^{high}$ and $hBK_{Ca}^{low}$ BC cells in response to TAM+M. Endoxifen significantly increased $DiBAC_4(3)$ fluorescence intensity in $hBK_{Ca}^{high}$, but not in $hBK_{Ca}^{low}$ BC cells, suggesting $\Psi_{PM}$ was more depolarized by TAM+M administration if $BK_{Ca}$ was expressed (Fig. 5, *D* and *F*). Further, $\Psi_{PM}$ was recorded during pharmacological inhibition of $BK_{Ca}$ with PAX, intracellular depletion of $Ca^{2+}$ by

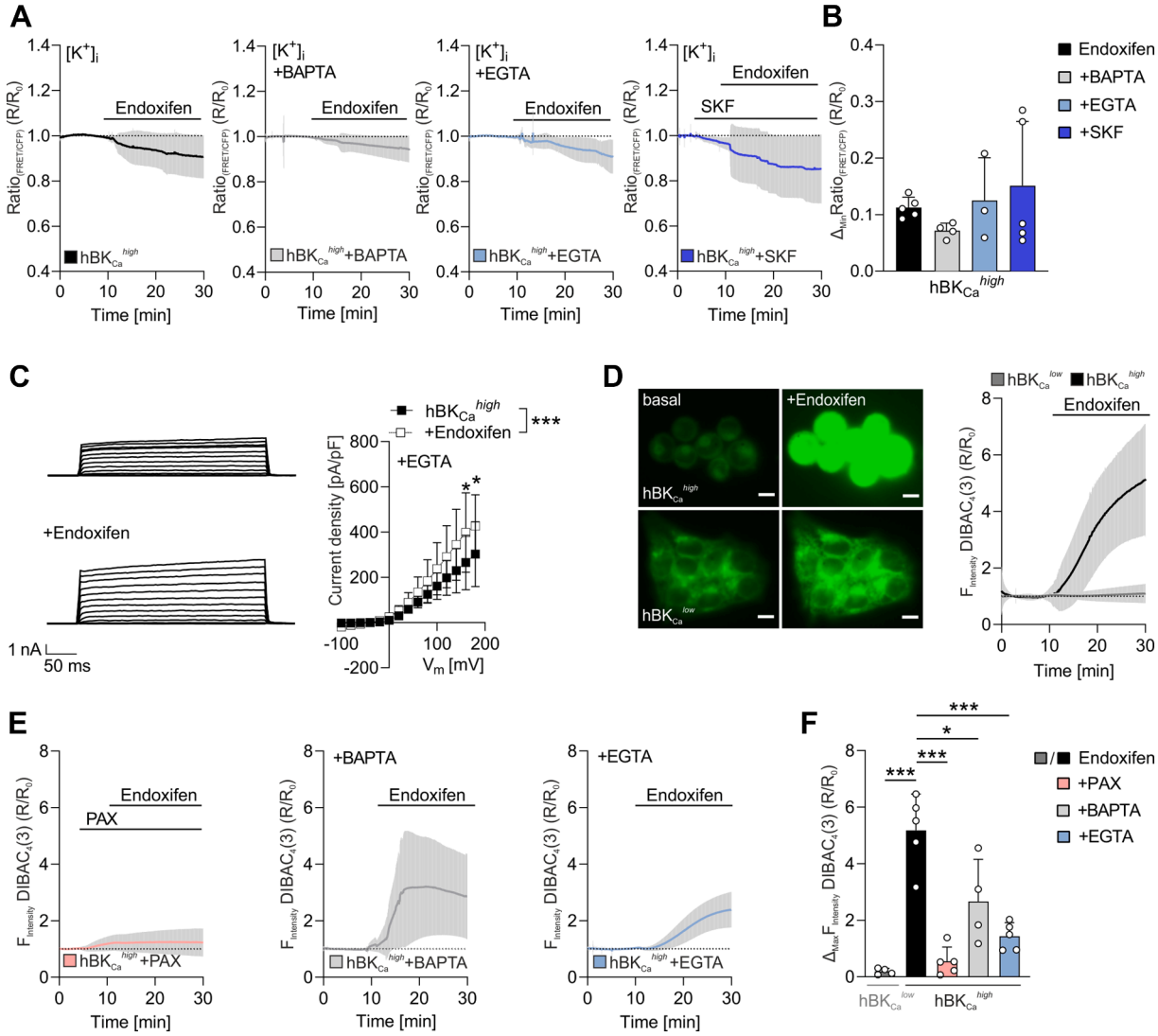


**Figure 5. The TAM+M-BK$_{Ca}$ channel axis, by modulating [K$^+$]$_i$, initiates intracellular Ca$^{2+}$ signals and a depolarized $\Psi_{PM}$ in BC cells.** *A*, FRET ratio signals of cytosolic $K^+$ changes over time and (*B*) statistical presentation of minimal (R) to basal ($R_0$) ratio ($\Delta_{Min}$) monitored in hBK$_{Ca}^{high}$ BC cells in presence of endoxifen (Fig. 2*D*, 1 μM endoxifen), depleted intracellular $Ca^{2+}$ by BAPTA AM (BAPTA), $Ca^{2+}$-free, EGTA-buffered extracellular conditions, and TRP/C, STIM/ORAI1 channel block by SKF-96365 (SKF) (from *left* to *right*). *C*, representative whole-cell current tracings (*left*) and current density-voltage curves (*right*) of hBK$_{Ca}^{high}$ BC cells in presence of EGTA before and after endoxifen administration. *D*, representative fluorescence images (basal (*left*), endoxifen (*middle*)) and fluorescence intensity signals recorded over time (*right*) from hBK$_{Ca}^{low}$ and hBK$_{Ca}^{high}$ BC cells loaded with the membrane potential ($\Psi_{PM}$)-sensitive dye $DiBAC_4(3)$ and administration of endoxifen. Scale bar = 10 μm. *E* fluorescence intensity signals of hBK$_{Ca}^{high}$ BC cells loaded with $\Psi_{PM}$-sensitive dye $DiBAC_4(3)$ in the presence of PAX+endoxifen, BAPTA AM+endoxifen and EGTA+endoxifen. *F*, quantification of endoxifen-induced maximal change ($\Delta_{Max}$) in $DiBAC_4(3)$ fluorescence intensity in hBK$_{Ca}^{low}$ and hBK$_{Ca}^{high}$ BC cells under recording conditions that are specified in (*D*, *E*). Data represents average ± SD. n(independent experiments) = (*A*, *B*) 3-5, (*C*) 7, (*D*, *E*, *F*) 4-5 with $^*p \le 0.05$, $^{**}p \le 0.01$, $^{***}p \le 0.001$. *B*, one-way ANOVA followed by Tukey's multiple comparisons test. *C*, two-way ANOVA followed by Šídák's multiple comparisons test. *F*, one-way ANOVA followed by Dunnett's multiple comparisons test. Statistical values are described in detail in Table S5.

BAPTA AM and $[Ca^{2+}]_{ex}$-free conditions with EGTA (Fig. 5, *E* and *F*). Again, increased fluorescence intensity indicated a more depolarized $\Psi_{PM}$, but this TAM+M-induced effect in hBK$_{Ca}^{high}$ cells was largely abrogated by pharmacological $BK_{Ca}$ inhibition and considerably reduced in the presence of the $Ca^{2+}$-chelators (Fig. 5*F*).

Combined, TAM+M influences $[K^+]_i$ dynamics by $BK_{Ca}$ activation, leading to depolarized $\Delta\Psi_{PM}$ and mobilization of intracellular and extracellular $Ca^{2+}$ sources to maintain $BK_{Ca}$ stimulation.

### *TAM+M increases single-channel currents in a Ca$^{2+}$-independent manner*

As our data suggests that the TAM+M-$BK_{Ca}$ axis includes mobilization of $Ca^{2+}$ from multiple stores, we applied inside-out patch-clamp recordings to study TAM+M-mediated $BK_{Ca}$ single channel behavior in the presence and absence of $Ca^{2+}$. Accordingly, we used hBK$_{Ca}^{high}$ BC cells to study the influence of endoxifen on channel open probability under $Ca^{2+}$-free conditions or at physiological $Ca^{2+}$ levels at either negative (-50 mV) or positive (+50 mV) voltages (Fig. 6, *A* and

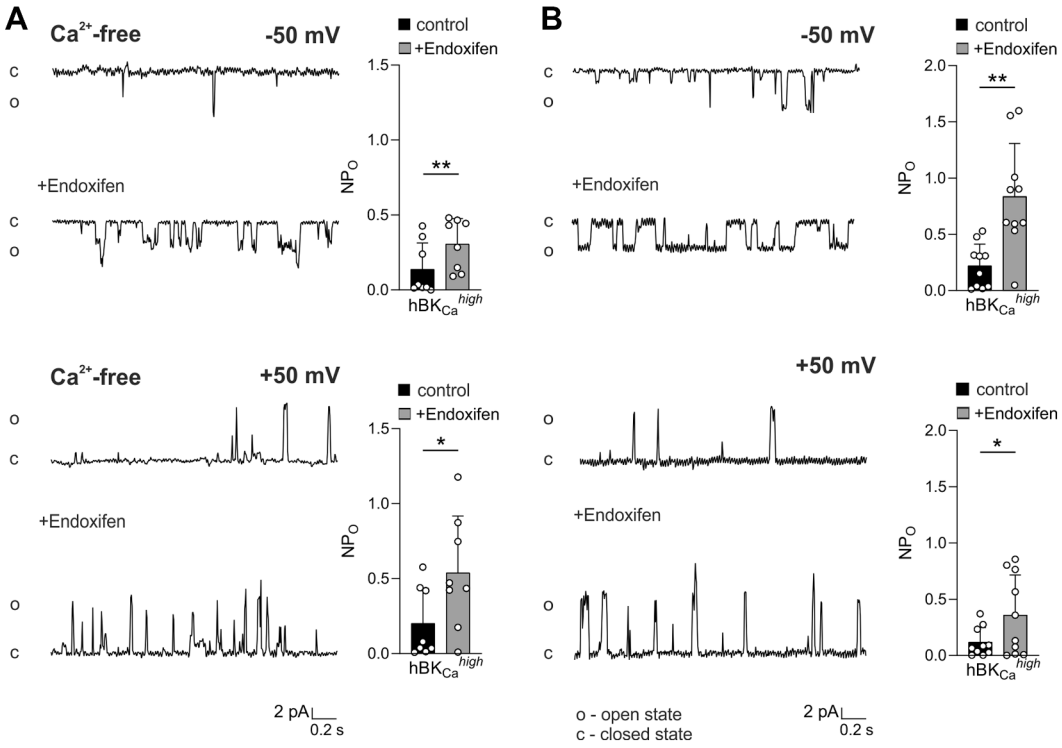


**Figure 6. TAM+M enhances single channel open probabilities independent of $Ca^{2+}$ levels**. *A* and *B*, representative single channel recordings (*left*) and corresponding bar charts (*right*) of $hBK_{Ca}^{high}$ BC cells at negative and positive voltages (-50 and +50 mV) using a symmetric isotonic KCl solution containing either (*A*) $Ca^{2+}$-free or (*B*) physiological $Ca^{2+}$ levels. 1 μM endoxifen significantly increased $BK_{Ca}$ open probability ($NP_O$) under all at investigated conditions. Data represents average ± SD. n (cells) = (*A*) 8 and (*B*) 10 with **p* ≤ 0.05 and ***p* ≤ 0.01. (*A*) Wilcoxon test. (*B*) Paired *t* test. Statistical values are described in detail in Table S6.

*B*). At both voltages and $Ca^{2+}$ levels, endoxifen increased the number of channel openings, resulting in a significantly increased open probability ($NP_O$). Single channel conductance yielded values of approximately 200 pS (data not shown), which is in the expected range of canonical $BK_{Ca}$ channels. As the effect of endoxifen on $NP_O$ was independent of $Ca^{2+}$, we conclude that TAM+M modulates $BK_{Ca}$ function through a direct interaction and not indirectly by influencing $Ca^{2+}$ handling mechanisms like transporters, channels or stores. Interestingly, the highest $NP_O$ in response to endoxifen was recorded at physiological $Ca^{2+}$ levels and negative potentials (Fig. 6*B*), supporting our initial hypothesis that TAM+M-mediated $BK_{Ca}$ activity results in a feed-forward mechanism, including $Ca^{2+}$-dependent sustained $BK_{Ca}$ channel activation.

In sum, these single-channel recordings confirmed TAM+M-promoted $BK_{Ca}$ channel activity in a voltage-and $Ca^{2+}$-independent manner. This suggests a direct interaction between TAM+M and $BK_{Ca}$ channels, which results in an increased channel open probability.

### *Molecular modelling of TAM+M interaction with hBK$_{Ca}$*

Docking of TAM+M against entire $hBK_{Ca}$ protein structures (PDB Codes 6V38, 6V22 (60)), suggest two putative extracellular binding sites, one located close to the N-terminus (termed "WDF", based on the amino acids forming major interactions with TAM+M) (Fig. 7, *A* and *B* and Fig. S3, *D* and *E*) and one posed between subunits close to the pore (termed "TSYF" based on the same principle) (Fig. 7, *C* and *D* and Fig. S3, *D* and *E*). Both pockets show high docking scores for 4-OH-TAM and endoxifen with virtually the same binding modes, indicating similar effects. The binding modes place the stilbene scaffolds in the hydrophobic part of the transmembrane region. They show π-π interactions with W22 and F252 for the "WDF" site, as well as with F131 and Y274 for the "TSYF" site. In the "WDF" site, the positively charged secondary or tertiary amines of endoxifen and 4-OH-TAM form a salt bridge to D261. Interestingly, in the "TSYF" site, the protonated tertiary amine of 4-OH-TAM appears to preferentially interact with the hydroxyl function of the side chain of S134, while the protonated secondary amine of endoxifen can, in principle, form two hydrogen bonds targeting the side chain hydroxyl group of S134 and the backbone carbonyl of F131. The phenolic hydroxyl functions of both metabolites are located in close proximity to the backbone of W23 ("WDF" site) or the backbone of T298 ("TSYF" site). In addition to the high docking scores in 6V38 (Fig. S3*D*), a homology model (Fig. S3*F*) showed the "WDF" binding site close to the recently described binding site of E2 in the structure of $BK_{Ca}$ with β1-subunit in smooth muscle cells (21).

In sum our results reveal that TAM+M activates $BK_{Ca}$ by potential binding sites in the α-subunit of $BK_{Ca}$ to trigger changes in the $[K^+]_i$ *vs* $[K^+]_{ex}$ balance that in turn allows

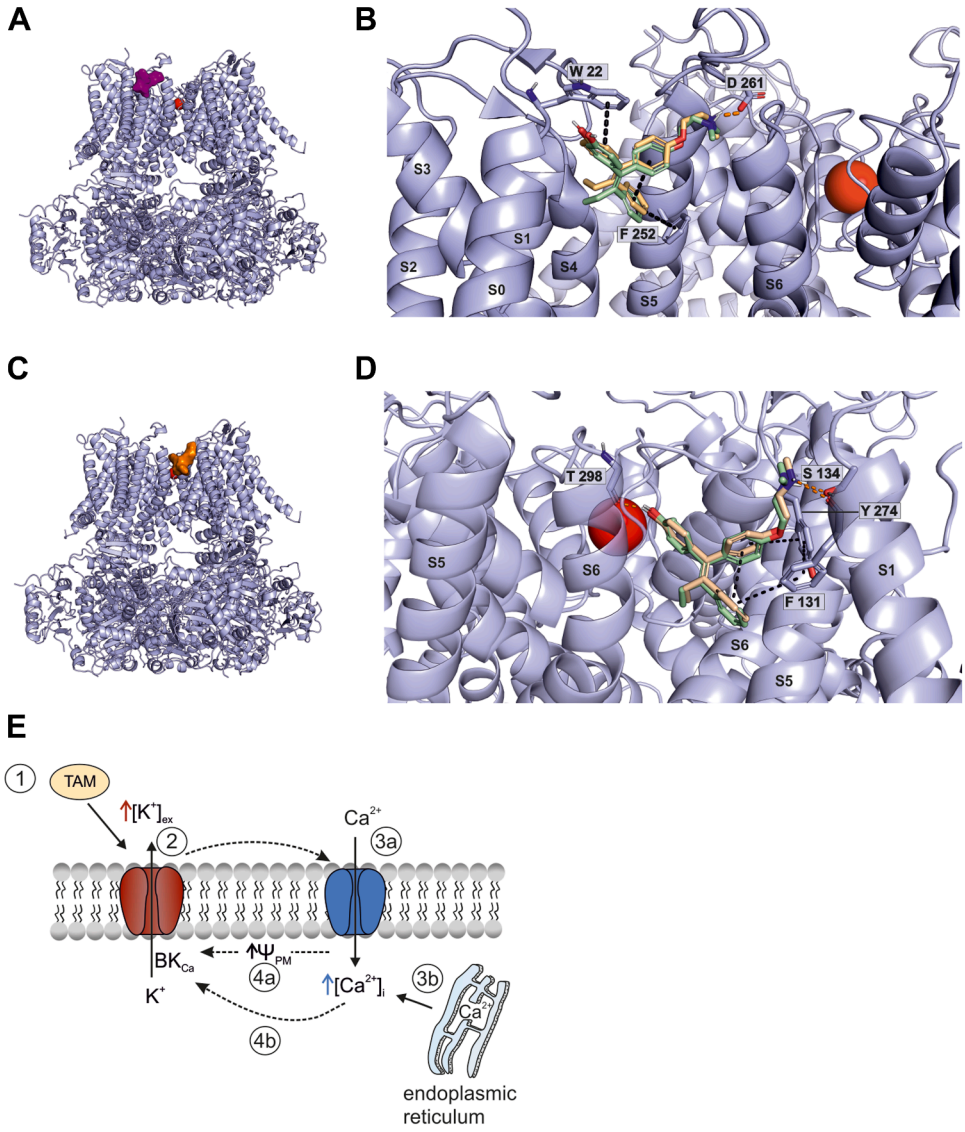


**Figure 7. Molecular modelling of TAM+M interaction with hBK$_{Ca}$.** Results of docking simulation of TAM+M into (*A*, *B*) extracellular binding pocket "WDF" and (*C*, *D*) pore-interacting binding pocket "TSYF" in (*A*, *C*) tetrameric arrangement of α-subunits and (*B*, *D*) magnified regions of putative binding modes in cryo-EM structures of $Ca^{2+}$-bound BK$_{Ca}$ (PDB 6V38) after induced fit docking. The high docking scores indicate strong hydrophobic, polar and π-π interactions at (*A*, *B*) segments S0-S5 with the amino acids W22, D261 and F252 and (*C*, *D*) S1, S5-S6 with T298, S134, Y274, F131. Color code: Segments, *light blue*; $K^+$, *red sphere*; Endoxifen, *yellow*; 4-OH-TAM, *green*. *E*, summarizing scheme of BK$_{Ca}$-mediated alterations in $K^+$ and $Ca^{2+}$ homeostasis due to TAM+M stimulating BK$_{Ca}$ channel activation. (1) TAM+M provoke BK$_{Ca}$ channel activity, (2) BK$_{Ca}$-dependent $K^+$ dynamics lead to an increased extracellular $K^+$ ($[K^+]_{ex}$) and a lower $[K^+]_i$; $Ca^{2+}$ entry through (3a) TRP/C-like $Ca^{2+}$ channels in the PM and (3b) by its release from intracellular stores such as the endoplasmic reticulum results in a cytosolic $Ca^{2+}$ accumulation ($[Ca^{2+}]_i$) in BC cells. This increase in $[Ca^{2+}]_i$ in turn causes (4a) voltage- and (4b) $Ca^{2+}$-dependent activation of BK$_{Ca}$, which is thus part of a feed-forward amplification mechanism in TAM+M exposed BC cells.

elevated $[Ca^{2+}]_i$ by facilitating $Ca^{2+}$ influx across the PM and by $Ca^{2+}$ release from the endoplasmic reticulum. $Ca^{2+}$ accumulation and depolarized $\Psi_{PM}$ subsequently maintain BK$_{Ca}$ activity in terms of a feed-forward mechanism (Fig. 7*E*).

## Discussion

We combined live-cell imaging with electrophysiological and pharmacological approaches in human and murine BC cell systems and obtained novel insights into the interaction of clinically relevant TAM+M with the "oncochannel" BK$_{Ca}$, a $K^+$ channel that is suspected to confer a negative influence on endocrine treatment in BC patients (9).

Supported by molecular docking calculations, our analyses of TAM+M-mediated effects in human and murine MMTV-PyMT-based BC cell models expressing either no, low, medium or high levels of BK$_{Ca}$ show a close correlation between the cells' BK$_{Ca}$ status and their response to endocrine agents.

We suggest that the TAM+M-BK$_{Ca}$ axis in BC cells directly controls the intracellular $K^+$ and $Ca^{2+}$ balance, as the observed effects of endocrine agents on ion homeostasis occurred within seconds or minutes and were limited to BK$_{Ca}$-proficient cells, and were independent from genomic actions of the ER. In fact, BK$_{Ca}$ but not ER status of the BC cells had an influence on whether TAM+M exposure caused a $K^+$ drop in the cells and consequently a $Ca^{2+}$ accumulation.

## TAM-$BK_{Ca}$ axis in BC cells

Our observed TAM+M-mediated activation of $BK_{Ca}$ in BC is consistent with our previous findings that low concentrations of TAM+M promote rather than inhibit BC cell growth in the presence of functional $BK_{Ca}$ channels (9). Accordingly, high *KCNMA1* expression levels resulted in lower recurrence-free survival rates in $ER^+$ BC patients (9). By quantifying $K^+$ channel transcripts from human $ER^+$ BC biopsies and human BC cells, we confirmed *KCNMA1* expression (7) is aberrantly increased in bulk tumor samples and selected BC cell lines.

When we validated the functional expression of $BK_{Ca}$ channels in our BC cell models, we observed a significant PAX-sensitive $K^+$ current component in $hBK_{Ca}^{medium}$ and $hBK_{Ca}^{high}$ cells that was not present in $hBK_{Ca}^{low}$ BC cells, thereby confirming previous reports of $BK_{Ca}$ expression in $hBK_{Ca}^{low/high}$ cell models (7, 9). In contrast, pharmacological modulation of $BK_{Ca}$ by the channel opener NS11021 led to an increase in current densities in whole-cell patch-clamp analysis and a drop in $[K^+]_i$, from which we conclude that human BC cells with varying $BK_{Ca}$ channel levels represent a suitable model to study the putative effects of TAM+M on $BK_{Ca}$ channel activity and ion homeostasis.

In this current work, we further established a correlation between the $BK_{Ca}$ expression level, the reduction of $[K^+]_i$ and the elevation in $[Ca^{2+}]_i$ in response to TAM+M. Our $BK_{Ca}^{rescue}$ experiments in $hBK_{Ca}^{low}$ BC cells confirmed TAM+M-mediated $BK_{Ca}$ activity by restoring $[K^+]_i$ dynamics. Additionally, we demonstrated that the "pore death" mutant $BK_{Ca}^{G354S}$ expressed in $hBK_{Ca}^{low}$ BC cells did not mediate TAM+M-provoked $[K^+]_i$ dynamics. These defined amendments in $BK_{Ca}$ expression and activity that we implemented either as $BK_{Ca}$-$RFP^{rescue}$ or $BK_{Ca}^{G354S}$ confirmed a direct interaction of TAM+M with the pore-forming α-subunit. Importantly, ER-independent actions of TAM are frequently reported, especially in the context of cancer cell proliferation (61–63), however, these have not been examined at the level of $K^+$ and $Ca^{2+}$ homeostasis.

In contrast to our previous observations where prolonged E2 exposure increased BC cell proliferation in a $BK_{Ca}$-dependent manner (9), our current work revealed that E2-mediated effects on $K^+$ dynamics were independent of BC $BK_{Ca}$ channels, at least during the few-minute time frame considered here. Thus, follow-up studies are required to address and explain these differences in the mode of action of E2 and TAM+M on $BK_{Ca}$. For the time being, we suggest that the $BK_{Ca}$-dependent pro-proliferative effects of E2 may be mediated by an alternative signaling pathway that is independent of any direct interaction between E2 and $BK_{Ca}$'s α-subunit or ER. This view is in line with findings in non-cancerous cells, where the expression of auxiliary β1-subunits was essential for the activation of $BK_{Ca}$ by E2 (18, 21, 22). It is also in line with findings in triple negative breast cancer cells (absence of ER, PR and HER2), where E2-dependent activation of G protein-coupled estrogen receptor 1 (GPER) stimulated a non-genomic pathway causing cell proliferation (64, 65). The role of $BK_{Ca}$ in this context, however, was not specifically investigated.

Interestingly, TAM+M-induced $[Ca^{2+}]_i$ dynamics were decreased by $[Ca^{2+}]_{i/ex}$-depleted conditions, TRP/C and SOCE inhibition and by $BK_{Ca}$ blockade with PAX, giving rise to the view that $BK_{Ca}$-mediated $K^+$ loss triggers $Ca^{2+}$ elevation. To this end, we showed that the presence of $[Ca^{2+}]_{i/ex}$ or intact SOCE is dispensable for the TAM+M-induced response of $BK_{Ca}$, as FRET recordings demonstrated an unaltered TAM+M-provoked $K^+$ efflux, whole-cell patch-clamp experiments showed increased current densities even under $Ca^{2+}$-free EGTA-buffered conditions, and the $NP_O$ of $BK_{Ca}$ in inside-out patches was raised independent of $Ca^{2+}$ stores or transporting mechanisms. It should be emphasized that physiological $Ca^{2+}$ conditions contributed to the highest increase in $NP_O$, confirming an amplified TAM+M effect on $BK_{Ca}$ activity by $Ca^{2+}$.

To address whether the TAM+M-$BK_{Ca}$ axis plays a role for intracellular $Ca^{2+}$ mobilization, we induced $Ca^{2+}$ mobilization from the endoplasmic reticulum by ATP. The $K^+$ loss induced by TAM+M caused an increase in $[Ca^{2+}]_i$ under $[Ca^{2+}]_{ex}$-depleted conditions, probably due to an increase in $Ca^{2+}$ driving force.

Hence, $BK_{Ca}$ gating in BC cells is also linked to the homeostasis of this intracellular $Ca^{2+}$ pool, and thus influences cellular signaling processes, as previously demonstrated for a wide range of different cell types (66). This is further corroborated by the PAX-induced $BK_{Ca}$ inhibition, which impaired a significant part of the ATP-elicited $[Ca^{2+}]_i$ transients after TAM+M pre-treatment (Fig. 4, *E* and *F*). These findings are in line with those previously reported by us, where PAX reduced the basal $[Ca^{2+}]_i$ levels in MDA-MB-453 BC cells, while the mean peak amplitude of the $[Ca^{2+}]_i$ signals induced by ATP remained unaltered (7).

We also considered that the TAM+M-$BK_{Ca}$ axis would affect the $\Psi_{PM}$ and thus voltage-dependent $BK_{Ca}$ activation in the presence and absence of $[Ca^{2+}]_{ex/i}$. Indeed, we triggered a strong $\Psi_{PM}$ depolarization with TAM+M that depended on the $BK_{Ca}$ status and was sensitive to genetic or pharmacological inhibition of the channel. The measured effects on $\Psi_{PM}$ were less prominent when $[Ca^{2+}]_i$ or $[Ca^{2+}]_{ex}$ were selectively depleted, indicating that $\Psi_{PM}$ depolarization is a consequence of the (initial) TAM+M-$BK_{Ca}$ interaction. Although this may be counterintuitive at first, as the $BK_{Ca}$-mediated $K^+$ efflux should cause a greater membrane polarization rather than depolarization, we need to be aware of, that $DiBAC_4(3)$ is a slow-acting voltage-sensitive dye (59). We conclude that we have not been able to demonstrate the initial and rapid hyperpolarizing effect of TAM+M, as only the subsequent $Ca^{2+}$ influx leading to membrane depolarization is detected by $DiBAC_4(3)$.

Finally, for the TAM+M binding sites suggested by molecular docking, additional homology modelling of the β1 subunit to the β4 subunit (in 6V22) revealed, that the extracellular "WDF" binding site would lie close to the amino acids W163 and F166 of the β1-subunit, which were found to be critical for the effect of E2 on $hBK_{Ca}$ channel complexes (21). Both binding sites are close to binding sites of the $BK_{Ca}$ channel activator CTIBD (4-(4-(4-chlorophenyl)-3-

(trifluoromethyl)isoxazol-5-yl)benzene-1,3-diol) (67, 68), with CTIBD occupying the same space as TAM+M in the "WDF" binding site. According to our simulations, both binding sites are located in the extracellular region, fitting well to the recently reported activation of $BK_{Ca}$ by a membrane-impermeable form of TAM in smooth muscle cells (69).

In conclusion, we show that TAM+M induces considerable changes in the $K^+$ and $Ca^{2+}$ homeostasis in human and murine BC. This is mediated by direct activation of $BK_{Ca}$ oncochannels. TAM+M binding to one or two postulated extracellular binding sites results in $BK_{Ca}$ activation, followed by the elevation of $[Ca^{2+}]_i$ and a more depolarized $\Psi_{PM}$. Both effects consequently lead to a sustained feed-forward mechanism of $BK_{Ca}$ activation. Considering that $BK_{Ca}$ is involved in cell cycle control, proliferation, invasion, migration and malignancy of BC cells, it may be inferred from these changes that in patients with BC they may affect the response to endocrine treatment and promote the development of drug treatment resistance. A future perspective for translation of our results into clinical practice should be the analysis of $BK_{Ca}$ channel expression in tumor biopsies, upfront onset of TAM therapy to predict TAM-modulation based on ER-independent interaction with oncochannels. In addition, we envision that the pharmacological inhibition of $BK_{Ca}$ could be promising as a novel therapeutic in targeted anti-cancer concept, either in patients with endocrine resistance, or in patients with BC having aberrant $BK_{Ca}$ channel expression.

## Experimental procedures

### Cell culture

Human BC cell lines MDA-MB-453 ($hBK_{Ca}^{high}$ ($ER^-$)), MCF-7 ($hBK_{Ca}^{low}$ ($ER^+$)), CAMA-1 ($hBK_{Ca}^{medium}$ ($ER^+$)), SKBr-3 ($hBK_{Ca}^{low}$ ($ER^-$)) were purchased from ATCC: The Global Bioresource Center. Cells were cultivated in Dulbecco's modified eagle's medium (DMEM), 10% fetal bovine serum (FBS) and 1% penicillin/streptomycin (P/S) (Thermo Fisher Scientific). MDA-MB-453 and MCF-7 were additionally supplemented with 1 mM sodium pyruvate (Thermo Fisher Scientific). Murine BC cells were isolated from breast tumor-bearing MMTV-PyMT transgenic FVB/N WT ($mBK_{Ca}^{WT}$) and BKKO ($mBK_{Ca}^{KO}$) mice (9). Animal experimental procedures were approved by the local ethics Committee for Animal Research (Regierungspräsidium Tübingen) and in accordance with the German Animal Welfare Act. Animals had access to food and water ad libitum and were kept on a 12 h light/dark-cycle under controlled humidity and temperature. Spontaneous tumor induction and development was monitored at an age of 12 to 14 weeks, and murine BC cells were isolated from n = 5 $mBK_{Ca}^{WT}$ and n = 6 $mBK_{Ca}^{KO}$ mice. Breast cancer cells were isolated from primary tumors as previously described (7, 70) and cultured in modified improved minimal essential medium (IMEM) supplemented with 5% FBS and 1% P/S. Human and murine BC cells were cultivated at 37 °C, 5% $CO_2$ in a humidified incubator.

Subculturing of cells was performed at 80 to 90% confluency with 0.05% trypsin-EDTA diluted in PBS (Thermo Fisher Scientific) for 5 min in the incubator. After centrifugation at 1000 rpm for 5 min, cells were seeded into new cell culture flasks or dishes for subsequent experiments. Cell culture materials were purchased from Sarstedt or Corning (Kaiserslautern, Germany). In experiments that aimed to exclude the influence of growth factors and hormones, cells were cultured 72 h in serum-free medium followed by charcoal-stripped serum (CCS) enriched medium.

### Electrophysiology

For whole-cell and excised inside-out patch-clamp experiments, 300,000 cells of $hBK_{Ca}^{medium/high}$ and 150,000 cells of $hBK_{Ca}^{low}$ were seeded in 35 mm dishes the day before measurement. For whole-cell patch-clamp experiments, BC cells were washed twice with pre-warmed PBS and extracellular buffer ($Bf_{ex}$) containing (in mM): 143 NaCl, 2 $CaCl_2$, 1 $MgCl_2$, 10 HEPES, 10 D-Glucose, pH 7.4 adjusted with NaOH (all from Carl Roth) was applied. A P-1000 Flaming/Brown micropipette puller (Sutter Instruments) was used to pull micropipettes with 3.5 to 4.5 MΩ from borosilicate glass capillaries (BM150–10P, Science Products GmbH, Hofheim, Germany). Glass micropipettes were polished using an MF-830 Micro Forge (Narishige International Ltd) and filled with intracellular solution (in mM: 130 K-gluconate, 10 KCl, 5 $MgCl_2$, 0.6 EGTA, 5 HEPES, 0.1 $CaCl_2$, 0.2 $Na_2$-GTP, 2.0 Mg-ATP, pH 7.4 adjusted with KOH). Osmolality of intra-and extracellular buffer was adjusted to 300 mOsm/kg. Single-channel recordings in excised inside-out patches were performed in symmetrical isotonic KCl buffer containing (in mM): 10 NaCl, 110 KCl, 2.69 $CaCl_2$, 5 EGTA, 2 $MgCl_2$, 10 HEPES, pH 7.4 adjusted with KOH to obtain physiological $[Ca^{2+}]_i$ levels (0.1 μM free $Ca^{2+}$) (71) and $Ca^{2+}$-free conditions were achieved by depleting $CaCl_2$. Micropipettes with 5.0 to 7.0 MΩ were pulled and polished as mentioned above. For both configurations, a Nikon Tc2R microscope equipped with a Nikon S Plan Fluor 40x/0.6 objective (Nikon Instruments Inc.) and a DFK 33U x 174 camera (The Imaging Source Europe GmbH) was used for visual guidance. The recording setup was further comprised of a MP-225 micromanipulator (Sutter Instruments) and an EPC10 amplifier (HEKA Elektronik GmbH). PatchMaster software (HEKA Elektronik GmbH) and nest-o-patch (http://sourceforge.net/projects/nestopatch, Dr V. Nesterov) were used for data recording and analysis. In whole-cell mode, currents were recorded in response to 300 ms voltage steps ranging from −100 to +180 mV ($hBK_{Ca}^{high}$) and −100 to +120 mV ($hBK_{Ca}^{low}$) in 20 mV increments from a holding potential of −40 mV. Recordings were repeated after addition of PAX (1 min), NS11021 (3 min) and TAM+M (8 min). Whole-cell capacity and access resistance were compensated. Cells for which access resistance changed by more than 20% during the recording were excluded from the analysis (<10%). The mean current amplitude during the last 16.2 ms of the depolarizing pulse was measured and normalized to cell capacity. Single-channel currents were recorded using voltage steps ranging from −80 to +80 mV in increments of 10 mV for 15 s.

Recordings were repeated after addition of TAM+M (5 min). For current analysis using Nest-o-Patch, the recordings were filtered at 500 Hz. The open probability from a group of channels ($NP_O$) in the patches represents channel activity. Representative single-channel recordings and analysis of $NP_O$ are described for −50 and +50 mV at physiological or $Ca^{2+}$-free conditions.

### FRET-based $K^+$ imaging

BC cells were seeded to a confluency of 70 to 80% on glass coverslips (1.5 H 30 mm, Paul Marienfeld GmbH) in 35 mm dishes (Corning). For FRET-based live-cell $K^+$ imaging, cells were transfected 16 h prior to the experiments with PolyJet (SignaGen Laboratories) according to the manufacturer's instructions. Plasmids used in this study are as follows: FRET-based $K^+$ sensor cytosolic lc-LysM GepII1.0 (40) as a gift from Roland Malli; $BK_{Ca}$ channel overexpression was performed with $BK_{Ca}$-RFP (7) as well as respective control by the empty RFP plasmid (72). Loss-of-function mutant $BK_{Ca}^{G354S}$ previously reported by (43), was generated by site-directed mutagenesis using: $BK_{Ca}$-RFP plasmid as template, the primers: $BK^{G354S}$ *forward* 5′-ACA ATG TCT ACA GTG AGT TAT GG-3′ and $BK^{G354S}$ *reverse* 5′-CAT AAA CGT CCC CAT AAC TCA-3′, Q5 High-Fidelity DNA Polymerase (NEB) followed by digestion with *Dpn*I (NEB) according to manufacturer's instructions. Plasmid preparation was performed by NucleoBond Xtra Maxi Kit according to the manufacturer's protocol (Macherey-Nagel). The successful mutagenesis was validated by sequencing of the insert (Microsynth SeqLab).

Glass coverslips were transferred to a perfusion chamber (NGFI GmbH, Graz, Austria) and washed twice with $Bf_{ex}$. To obtain intracellular $Ca^{2+}$-depleted conditions, BC cells were incubated for 30 min prior to the recording with cell-permeant BAPTA-acetoxymethyl ester (BAPTA AM). Extracellular $Ca^{2+}$-free conditions were achieved by the addition of EGTA (Sigma-Aldrich) and omission of $CaCl_2$. Measurements were performed under the presence of different compounds with stock solutions diluted in DMSO at the following final concentrations: 1 μM endoxifen, 1 μM 4-OH-TAM (Sigma-Aldrich), 10 μM NS11021, 5 μM paxilline, 10 μM SKF-96365 (Tocris). Dilution series were performed with 1 μM endoxifen and 1 μM 4-OH-TAM to perform concentration-dependent experiments. Controls were treated with DMSO.

A Zeiss Axio Observer Z1 (Carl Zeiss AG) microscope was used for FRET-based measurements as previously described (7, 70, 73). The imaging platform contained a BioPrecision2 automatic XY-Table (Ludl Electronic Products, Ltd) and a Plan-Neofluar 40x/1,30 Oil immersion objective (Carl Zeiss AG). An external light source (LED-Hub, Omicron Laserage) equipped with LED at 340 nm, 380 nm, 455 nm, 470 nm and 505 to 600 nm and emission filters: 340x, 380x, 427/10, 473/10 and 575/15 (AHF, Analysentechnik) allowed live-cell imaging by FRET. For FRET measurements, an Optosplit II (Cairn Research) together with dichroic mirrors (459/526/596 nm) and emission filters (475/543/702 nm) was utilized for simultaneous recording of FRET and CFP emissions (all from AHF Analysentechnik). Images were captured by a pco.panda 4.2 bi sCMOS camera (Excelitas PCO) and VisiView software (Visitron Systems). Addition of buffers and treatments was enabled by a gravity-based perfusion system (NGFI GmbH).

### Fura-2-based $Ca^{2+}$ measurement

For the Fura-2 recordings, the BC cells were seeded 24 h before the measurement with a confluence of 50% on glass cover slips in 35 mm dishes. Stocks of 15% Pluronic F-127 (Sigma-Aldrich) and 1 mM Fura-2 AM (Biomol GmbH, Hamburg, Germany) were mixed in a 1:3 dilution (following Fura-2). BC cells were washed with $Bf_{ex}$ and loaded for 20 min at RT with a final concentration of 3.3 μM Fura-2 AM. Subsequently, cells were washed with $Bf_{ex}$ for 10 min at RT. Imaging was performed on a Zeiss Axiovert 200M microscope equipped with a 40x Fluar 1.30 oil immersion objective (Carl Zeiss AG). Further, illumination was provided by a *p*E-$340^{fura}$ LED (CoolLED), together with excitation filters 340/26 and 380/14 (AHF Analysentechnik). Dichroic mirror 515LP and emission filter 525/15 (AHF Analysentechnik) enabled specific detection of Fura-2 based $Ca^{2+}$ signals. A pco.panda 4.2 sCMOS camera (Excelitas PCO) and VisiView were used for image acquisition. Perfusion of treatments was achieved by a gravity-based system. Next to already mentioned treatments, 100 μM ATP (Carl Roth) was applied.

### Plasma membrane potential measurements

Bis-(1,3-dibutylbarbituric acid)Trimethine Oxonol ($DiBAC_4(3)$) (Thermo Fisher Scientific) was used in a concentration of 0.25 μg/ml to determine $\Delta\Psi_{PM}$. BC cells were seeded on 30 mm glass cover slips, washed with $Bf_{ex}$ and incubated with $DiBAC_4(3)$ for 35 min at RT. During the measurement at the microscope Zeiss Axio Observer Z1, $DiBAC_4(3)$ was constantly present in the buffer. Excitation was performed by 470 nm LED and a dichroic mirror (409/493/573/652 nm), and an emission filter (514/605/730 nm) enabled $DiBAC_4(3)$ specific recordings.

### qRT-PCR

Gene expression levels of $BK_{Ca}$ subunits in human BC cells were analyzed using total mRNA isolated from $hBK_{Ca}^{low}$, $hBK_{Ca}^{medium}$ and $hBK_{Ca}^{high}$ BC cells. BC cells were seeded to a confluency of 80% in 100 mm dishes. Isolation, cDNA synthesis and qRT-PCR were performed as previously described (74). RNA was isolated using the NucleoSpin RNA kit (Macherey-Nagel) followed by cDNA synthesis of 0.5 μg RNA using iScript cDNA synthesis kit (Bio-Rad) according to manufacturer's instructions, respectively. SsoAdvanced Universal SYBR Green Supermix (Bio-Rad) and target-specific primer pairs were used to perform qRT-PCR with CFX Connect Real-Time PCR Detection System (Bio-Rad).

### Human breast cancer biopsies and nanostring nCounter gene expression analysis

An endocrine treatment study of 1286 BC patients between 2005 and 2011 (German Clinical Trial Register DRKS

00000605, "IKP211" study) was previously described for the analysis of 551 primary tumor biopsies from hormone receptor positive, post-menopausal patients with Nanostring nCounter gene expression analysis (7). In brief, patients were treated by TAM, aromatase inhibitor or switched endocrine therapy in between. Total RNA was isolated from FFPE tissues (Quick-DNA/RNA FFPE, ZymoResearch, Freiburg, Germany) of their breast cancer biopsies. Target-specific capture probes and color-coded reporter sets for ion channel genes and accessory subunits were designed and hybridized with 250 ng RNA in a thermal cycler at 65 °C for 20 h. The Nanostring nCounter system was used to measure fluorescence counts. Data analysis was performed with nSolver 4.0. Normalization to five housekeeping genes (*ABCF1*, *NRDE2*, *POLR2A*, *PUM1*, and *SF3A1*) was performed and cut off of log2 expression count was set to 5.5. We have previously published some information on the BC patient-related $BK_{Ca}$ channel expression profile in (7).

### Molecular docking simulation

TAM+M were docked against two protein cryo-EM structures of $BK_{Ca}$ under $Ca^{2+}$-bound and $Ca^{2+}$-bound in complex with the β4 subunit conditions (PDB Codes 6V38, 6V22, respectively, (60)) using Schrödingers software suite (Schrödinger Release 2024–4). Using the Protein Preparation Wizard (75), bond orders were reassigned, hydrogens replaced and sensible protonation states at pH 7.4 were determined using PROPKA. Each protein was subjected to a restrained minimization using the OPLS4 force field (76) and a 0.3 Å RMSD convergence criterion. Ligands were prepared using LigPrep at pH 7.0. We used SiteMap (77, 78) with shallow settings to identify a multitude of binding sites and split large binding sites using the DBSCAN clustering algorithm. This resulted in 277 and 368 potential binding sites for $BK_{Ca}$ under $Ca^{2+}$-bound and $Ca^{2+}$-bound in complex with β4 conditions, respectively. TAM+M were docked into each binding site using GLIDE (79) with standard precision. After the identification of putative binding sites, the extended induced fit docking protocol (80, 81) with extra precision in the structure of $BK_{Ca}$-$Ca^{2+}$-bound (6V38) was performed. For the refinement step, an implicit membrane was defined based on the experimental data.

### Statistical analysis

Statistical analysis was performed with GraphPad Prism 9 software (GraphPad, Software). All data were tested for outlier. Normal distribution was verified using Shapiro-Wilk or Kolmogorov-Smirnov test. If the variances of the populations were comparable, a two-tailed Unpaired *t* test was used; if F-test was significantly different, Welch's test was applied for the statistical comparison of normally distributed data. Normally distributed data of paired measurements were evaluated with Paired *t* test, while the Wilcoxon-test was used for non-normally distributed data. For the comparison of >2 groups either One-way ANOVA followed by Dunnett's or Tukey's multiple comparisons for normally distributed data was used, always considering F-test variances, or Two-way ANOVA followed by Dunnett's, Šídák's or Tukey's multiple comparisons test was performed. If data were not normally distributed, a Kruskal-Wallis test followed by Dunn's multiple comparisons test was performed. Statistical tests are indicated in the Figure legends and described in detail in the Supplementary Tables (Tables S1–S9). *p*-values of ≤ 0.05 were considered as statistically significant with $^{*}p \le 0.05$, $^{**}p \le 0.01$ and $^{***}p \le 0.001$.

## Data availability

All data are present in the article or the Supporting Information.

*Supporting information*—This article contains supporting information (7, 9, 21, 44, 82).

*Acknowledgments*—The authors thank Leonie Tumminello for excellent technical support.

*Author contributions*—S. M., W. S., F. M., L. M., A. T., and J. D. investigation; S. M., F. M., L. M., He. B., F. A. B., and F. M. B. formal analysis; S. M., W. S., F. M., L. M., He. B., D. S., L. B., M. C. S., F. A. B., and R. L. methodology; S. M. and R. L. validation; S. M., F. M., and F. A. B. data curation; S. M., F. M., L. M., A. T., F. A. B., and R. L. visualization; S. M. and R. L. writing–original draft; W. S., Hi. B., M. S., and R. L. conceptualization; W. S. and R. L. supervision; W. S., F. M., L. M., D. S., L. B., Hi. B., F. M. B., and M. S. writing–review & editing; He. B., D. G., I. B., F. F., F. M. B., M. S., and R. L. resources; F. M. B. software; W. S., Hi. B., M. S., and R. L. funding acquisition.

*Funding and additional information*—This work was funded by the Deutsche Forschungsgemeinschaft (DFG) with individual grants to R. L. L. B., M. C. S. and R. L. are members of the GRK2381: "cGMP: From Bedside to Bench", DFG grant number 335549539. S. M., W. S., Hi. B., M. S. and R. L. acknowledge financial support from the ICEPHA Graduate Program "Membrane-associated Drug Targets in Personalized Cancer Medicine". He. B. is a fellow of the Austrian Science Fund (FWF) funded Erwin-Schrödinger-Program, project number J-4457. M. S. and Hi. B. are supported by the DFG under Germany's Excellence Strategy – EXC 2180 to 390900677. F. M. and F. M. B. acknowledge support from the state of Baden–-Württemberg through bwHPC and the DFG through Grant No. INST 40/575-1 FUGG (JUSTUS 2 cluster). In addition, support is acknowledged from the High Performance and Cloud Computing Group at the Zentrum für Datenverarbeitung of the University of Tübingen and the DFG through Grant No. INST 37/935-1 FUGG (BinAC cluster). S. M., W. S., F. A. B., Hi. B. and M. S. are in part supported by the Robert Bosch Stiftung, Stuttgart, Germany.

*Conflict of interest*—The authors declare that they do not have any conflicts of interest with the content of this article.

*Abbreviations*—The abbreviations used are: ATP, adenosin-5′-triphosphate; BC, breast cancer; $BK_{Ca}$, voltage- and $Ca^{2+}$-activated $K^+$ channel of large conductance; CCS, charcoal-stripped serum; ER, estrogen receptor; HER2, human epidermal growth factor receptor; IF, immunofluorescence; $IP_3$, inositol-triphosphate; MMTV, mouse mammary tumor virus; PM, plasma membrane;

PyMT, polyoma middle T antigen; SOCE, store-operated $Ca^{2+}$ entry; TAM, tamoxifen; TAM+M, tamoxifen and its metabolite; TNBC, triple-negative BC.

## References


1. Bray, F., Laversanne, M., Sung, H., Ferlay, J., Siegel, R. L., Soerjomataram, I., *et al.* (2024) Global cancer statistics 2022: GLOBOCAN estimates of incidence and mortality worldwide for 36 cancers in 185 countries. *A Cancer J. Clin.* **74**, 229–263
2. Shaath, H., Elango, R., and Alajez, N. M. (2021) Molecular classification of breast cancer utilizing long non-coding RNA (lncRNA) transcriptomes identifies novel diagnostic lncRNA panel for triple-negative breast cancer. *Cancers* **13**, 5350
3. Harbeck, N., and Gnant, M. (2017) Breast cancer. *Lancet* **389**, 1134–1150
4. Perou, C. M., Sorlie, T., Eisen, M. B., van de Rijn, M., Jeffrey, S. S., Rees, C. A., *et al.* (2000) Molecular portraits of human breast tumours. *Nature* **406**, 747–752
5. Wu, S. Z., Al-Eryani, G., Roden, D. L., Junankar, S., Harvey, K., Andersson, A., *et al.* (2021) A single-cell and spatially resolved atlas of human breast cancers. *Nat. Genet.* **53**, 1334–1347
6. Huang, X., and Jan, L. Y. (2014) Targeting potassium channels in cancer. *J. Cell. Biol.* **206**, 151–162
7. Bischof, H., Maier, S., Koprowski, P., Kulawiak, B., Burgstaller, S., Jasińska, J., *et al.* (2024) mitoBK(Ca) is functionally expressed in murine and human breast cancer cells and potentially contributes to metabolic reprogramming. *Elife* **12**, RP92511
8. Dupuy, M., Gueguinou, M., Potier-Cartereau, M., Lézot, F., Papin, M., Chantôme, A., *et al.* (2023) SKCa- and Kv1-type potassium channels and cancer: promising therapeutic targets? *Biochem. Pharmacol.* **216**, 115774
9. Mohr, C. J., Schroth, W., Mürdter, T. E., Gross, D., Maier, S., Stegen, B., *et al.* (2022) Subunits of BK channels promote breast cancer development and modulate responses to endocrine treatment in preclinical models. *Br. J. Pharmacol.* **179**, 2906–2924
10. Ge, L., Hoa, N. T., Wilson, Z., Arismendi-Morillo, G., Kong, X. T., Tajhya, R. B., *et al.* (2014) Big potassium (BK) ion channels in biology, disease and possible targets for cancer immunotherapy. *Int. Immunopharmacol.* **22**, 427–443
11. Oeggerli, M., Tian, Y., Ruiz, C., Wijker, B., Sauter, G., Obermann, E., *et al.* (2012) Role of KCNMA1 in breast cancer. *PLoS One* **7**, e41664
12. Khaitan, D., Sankpal, U. T., Weksler, B., Meister, E. A., Romero, I. A., Couraud, P.-O., *et al.* (2009) Role of KCNMA1gene in breast cancer invasion and metastasis to brain. *BMC Cancer* **9**, 258
13. Ganser, K., Klumpp, L., Bischof, H., Lukowski, R., Eckert, F., and Huber, S. M. (2021) Potassium channels in cancer. *Handb Exp. Pharmacol.* **267**, 253–275
14. Ramírez, A., Vera, E., Gamboa-Domínguez, A., Lambert, P., Gariglio, P., and Camacho, J. (2018) Calcium-activated potassium channels as potential early markers of human cervical cancer. *Oncol. Lett.* **15**, 7249–7254
15. Bloch, M., Ousingsawat, J., Simon, R., Schraml, P., Gasser, T. C., Mihatsch, M. J., *et al.* (2007) KCNMA1 gene amplification promotes tumor cell proliferation in human prostate cancer. *Oncogene* **26**, 2525–2534
16. Liu, X., Chang, Y., Reinhart, P. H., Sontheimer, H., and Chang, Y. (2002) Cloning and characterization of glioma BK, a novel BK channel isoform highly expressed in human glioma cells. *J. Neurosci.* **22**, 1840–1849
17. Zuccolini, P., Gavazzo, P., and Pusch, M. (2022) BK channel in the physiology and in the cancer of pancreatic duct: impact and reliability of BK openers. *Front. Pharmacol.* **13**, 906608
18. Coiret, G., Matifat, F., Hague, F., and Ouadid-Ahidouch, H. (2005) 17-β-Estradiol activates maxi-K channels through a non-genomic pathway in human breast cancer cells. *FEBS Lett.* **579**, 2995–3000
19. Gonzalez-Perez, V., and Lingle, C. J. (2019) Regulation of BK channels by beta and gamma subunits. *Annu. Rev. Physiol.* **81**, 113–137
20. Cox, D. H., and Aldrich, R. W. (2000) Role of the beta1 subunit in large-conductance $Ca^{2+}$-activated $K^+$ channel gating energetics. Mechanisms of enhanced $Ca^{2+}$ sensitivity. *J. Gen. Physiol.* **116**, 411–432
21. Granados, S. T., Castillo, K., Bravo-Moraga, F., Sepúlveda, R. V., Carrasquel-Ursulaez, W., Rojas, M., *et al.* (2019) The molecular nature of the 17β-Estradiol binding site in the voltage- and Ca(2+)-activated K(+) (BK) channel β1 subunit. *Sci. Rep.* **9**, 9965
22. Valverde, M. A., Rojas, P., Amigo, J., Cosmelli, D., Orio, P., Bahamonde, M. I., *et al.* (1999) Acute activation of Maxi-K channels (hSlo) by estradiol binding to the beta subunit. *Science* **285**, 1929–1931
23. Coiret, G., Borowiec, A. S., Mariot, P., Ouadid-Ahidouch, H., and Matifat, F. (2007) The antiestrogen tamoxifen activates BK channels and stimulates proliferation of MCF-7 breast cancer cells. *Mol. Pharmacol.* **71**, 843–851
24. Dick, G. M., Rossow, C. F., Smirnov, S., Horowitz, B., and Sanders, K. M. (2001) Tamoxifen activates smooth muscle BK channels through the regulatory β1 subunit. *J. Biol. Chem.* **276**, 34594–34599
25. Dick, G. M., and Sanders, K. M. (2001) (Xeno)estrogen sensitivity of smooth muscle BK channels conferred by the regulatory beta1 subunit: a study of beta1 knockout mice. *J. Biol. Chem.* **276**, 44835–44840
26. Duncan, R. K. (2005) Tamoxifen alters gating of the BK α subunit and mediates enhanced interactions with the avian β subunit. *Biochem. Pharmacol.* **70**, 47–58
27. So, C. L., Saunus, J. M., Roberts-Thomson, S. J., and Monteith, G. R. (2019) Calcium signalling and breast cancer. *Semin. Cell. Dev. Biol.* **94**, 74–83
28. Zhang, W., Couldwell, W. T., Song, H., Takano, T., Lin, J. H. C., and Nedergaard, M. (2000) Tamoxifen-induced enhancement of calcium signaling in glioma and MCF-7 breast cancer Cells. *Cancer Res.* **60**, 5395–5400
29. Chu, S.-T., Huang, C.-C., Huang, C.-J., Cheng, J.-S., Chai, K.-L., Cheng, H.-H., *et al.* (2007) Tamoxifen-induced $[Ca^{2+}]_i$ rises and $Ca^{2+}$-Independent cell death in human oral cancer Cells. *J. Recept Signal. Transduct. Res.* **27**, 353–367
30. Hasegawa, G., Akatsuka, K., Nakashima, Y., Yokoe, Y., Higo, N., and Shimonaka, M. (2018) Tamoxifen inhibits the proliferation of non-melanoma skin cancer cells by increasing intracellular calcium concentration. *Int. J. Oncol.* **53**, 2157–2166
31. Kim, J.-A., Kang, Y. S., Jung, M.-W., Lee, S. H., and Lee, Y. S. (1999) Involvement of $Ca^{2+}$ influx in the mechanism of tamoxifen-induced apoptosis in HepG2 human hepatoblastoma cells. *Cancer Lett.* **147**, 115–123
32. Jan, C.-R., Cheng, J.-S., Chou, K.-J., Wang, S.-P., Lee, K. C., Tang, K.-Y., *et al.* (2000) Dual effect of tamoxifen, an anti-breast-cancer drug, on intracellular Ca2+ and cytotoxicity in intact cells *Toxicology and. Appl. Pharmacol.* **168**, 58–63
33. Dobrydneva, Y., Weatherman, R. V., Trebley, J. P., Morrell, M. M., Fitzgerald, M. C., Fichandler, C. E., *et al.* (2007) Tamoxifen stimulates calcium entry into human platelets. *J. Cardiovasc. Pharmacol.* **50**, 380–390
34. Rothberg, B. S. (2012) The BK channel: a vital link between cellular calcium and electrical signaling. *Protein. Cell* **3**, 883–892
35. Li, B., Jie, W., Huang, L., Wei, P., Li, S., Luo, Z., *et al.* (2014) Nuclear BK channels regulate gene expression via the control of nuclear calcium signaling. *Nat. Neurosci.* **17**, 1055–1063
36. Ledoux, J., Werner, M. E., Brayden, J. E., and Nelson, M. T. (2006) Calcium-activated potassium channels and the regulation of vascular tone. *Physiology (Bethesda)* **21**, 69–78
37. Shah, K. R., Guan, X., and Yan, J. (2021) Structural and functional coupling of calcium-activated BK channels and calcium-permeable channels within nanodomain signaling complexes. *Front Physiol.* **12**, 796540
38. Chubinskiy-Nadezhdin, V. I., Sudarikova, A. V., Shilina, M. A., Vasileva, V. Y., Grinchuk, T. M., Lyublinskaya, O. G., *et al.* (2019) Cell cycle-dependent expression of Bk channels in human mesenchymal endometrial stem cells. *Sc. Rep.* **9**, 4595
39. Ouadid-Ahidouch, H., Roudbaraki, M., Ahidouch, A., Delcourt, P., and Prevarskaya, N. (2004) Cell-cycle-dependent expression of the large $Ca^{2+}$-activated $K^+$ channels in breast cancer cells. *Biochem. Biophys. Res. Commun.* **316**, 244–251
40. Bischof, H., Rehberg, M., Stryeck, S., Artinger, K., Eroglu, E., Waldeck-Weiermair, M., *et al.* (2017) Novel genetically encoded fluorescent probes enable real-time detection of potassium in vitro and in vivo. *Nat. Commun.* **8**, 1422

41. Moldenhauer, H. J., Tammen, K., and Meredith, A. L. (2024) Structural mapping of patient-associated KCNMA1 gene variants. *Biophys. J.* **123**, 1984–2000
42. Boiteux, C., Posson, D. J., Allen, T. W., and Nimigean, C. M. (2020) Selectivity filter ion binding affinity determines inactivation in a potassium channel. *Proc. Natl. Acad. Sci. U. S. A.* **117**, 29968–29978
43. Du, X., Carvalho-de-Souza, J. L., Wei, C., Carrasquel-Ursulaez, W., Lorenzo, Y., Gonzalez, N., *et al.* (2020) Loss-of-function BK channel mutation causes impaired mitochondria and progressive cerebellar ataxia. *Proc. Natl. Acad. Sci. U. S. A.* **117**, 6023–6034
44. Bischof, H., Burgstaller, S., Vujic, N., Madl, T., Kratky, D., Graier, W. F., *et al.* (2019) Purification and application of genetically encoded potassium ion indicators for quantification of potassium ion concentrations within biological samples. *Curr. Protoc. Chem. Biol.* **11**, e71
45. Zúñiga, L., Cayo, A., González, W., Vilos, C., and Zúñiga, R. (2022) Potassium channels as a target for cancer therapy: current perspectives. *Onco Targets Ther.* **15**, 783–797
46. Prevarskaya, N., Skryma, R., and Shuba, Y. (2010) Ion channels and the hallmarks of cancer. *Trends Mol. Med.* **16**, 107–121
47. Pardo, L. A., and Stühmer, W. (2014) The roles of $K^+$ channels in cancer. *Nat. Rev. Cancer* **14**, 39–48
48. Ouadid-Ahidouch, H., and Ahidouch, A. (2013) $K^+$ channels and cell cycle progression in tumor cells. *Front. Physiol.* **4**, 220
49. Chen, Y. F., Lin, P. C., Yeh, Y. M., Chen, L. H., and Shen, M. R. (2019) Store-operated $Ca^{(2+)}$ entry in tumor progression: from molecular mechanisms to clinical implications. *Cancers (Basel)* **11**, 899
50. Merritt, J. E., Armstrong, W. P., Benham, C. D., Hallam, T. J., Jacob, R., Jaxa-Chamiec, A., *et al.* (1990) SK&F 96365, a novel inhibitor of receptor-mediated calcium entry. *Biochem. J.* **271**, 515–522
51. Rychkov, G., and Barritt, G. J. (2007) TRPC1 $Ca^{2+}$-Permeable channels in animal cells. In: Flockerzi, V., Nilius, B., eds. *Transient Receptor Potential (TRP) Channels*, Springer Berlin Heidelberg, Berlin, Heidelberg: 23–52
52. Zhang, J., Wei, J., He, Q., Lin, Y., Liang, R., Ye, J., *et al.* (2015) SKF95365 induces apoptosis and cell-cycle arrest by disturbing oncogenic Ca(2+) signaling in nasopharyngeal carcinoma cells. *Onco Targets Ther.* **8**, 3123–3133
53. Leung, Y.-M., Kwan, C.-Y., and Loh, T.-T. (1996) Dual effects of SK&F 96365 in human leukemic HL-60 cells: inhibition of calcium entry and activation of a novel cation influx pathway. *Biochem. Pharmacol.* **51**, 605–612
54. Jan, C. R., Ho, C. M., Wu, S. N., and Tseng, C. J. (1999) Multiple effects of 1-[β-[3-(4-methoxyphenyl)propoxy]-4-methoxyphenethyl]-1H-imidazole hydrochloride (SKF 96365) on $Ca^{2+}$ signaling in MDCK cells: depletion of thapsigargin-sensitive $Ca^{2+}$ store followed by capacitative $Ca^{2+}$ entry, activation of a direct $Ca^{2+}$ entry, and inhibition of thapsigargin-induced capacitative $Ca^{2+}$ entry *naunyn-schmiedeberg's. Arch. Pharmacol.* **359**, 92–101
55. Song, M., Chen, D., and Yu, S. P. (2014) The TRPC channel blocker SKF 96365 inhibits glioblastoma cell growth by enhancing reverse mode of the $Na^+/Ca^{2+}$ exchanger and increasing intracellular $Ca^{2+}$. *Br. J. Pharmacol.* **171**, 3432–3447
56. Decuypere, J. P., Monaco, G., Missiaen, L., De Smedt, H., Parys, J. B., and Bultynck, G. (2011) IP(3) receptors, Mitochondria, and ca signaling: implications for aging. *J. Aging Res.* **2011**, 920178
57. Müller, C. E., Baqi, Y., and Namasivayam, V. (2020) Agonists and antagonists for purinergic receptors. *Methods Mol. Biol.* **2041**, 45–64
58. Salter, M. W., and Hicks, J. L. (1995) ATP causes release of intracellular $Ca^{2+}$ via the phospholipase C beta/IP3 pathway in astrocytes from the dorsal spinal cord. *J. Neurosci.* **15**, 2961–2971
59. Bräuner, T., Hülser, D. F., and Strasser, R. J. (1984) Comparative measurements of membrane potentials with microelectrodes and voltage-sensitive dyes. *Biochim. Biophys. Acta* **771**, 208–216
60. Tao, X., and MacKinnon, R. (2019) Molecular structures of the human Slo1 $K^+$ channel in complex withβ4. *eLife* **8**, e51409
61. Charlier, C., Chariot, A., Antoine, N., Merville, M. P., Gielen, J., and Castronovo, V. (1995) Tamoxifen and its active metabolite inhibit growth of estrogen receptor-negative MDA-MB-435 cells. *Biochem. Pharmacol.* **49**, 351–358
62. Todorova, V. K., Kaufmann, Y., Luo, S., and Klimberg, V. S. (2011) Tamoxifen and raloxifene suppress the proliferation of estrogen receptor-negative cells through inhibition of glutamine uptake. *Cancer Chemother. Pharmacol.* **67**, 285–291
63. Lee, T. H., Chuang, L. Y., and Hung, W. C. (1999) Tamoxifen induces p21WAF1 and p27KIP1 expression in estrogen receptor-negative lung cancer cells. *Oncogene* **18**, 4269–4274
64. Yu, T., Liu, M., Luo, H., Wu, C., Tang, X., Tang, S., *et al.* (2014) GPER mediates enhanced cell viability and motility via non-genomic signaling induced by 17β-estradiol in triple-negative breast cancer cells *J Steroid. Biochem. Mol. Biol.* **143**, 392–403
65. van Barele, M., Heemskerk-Gerritsen, B. A. M., Louwers, Y. V., Vastbinder, M. B., Martens, J. W. M., Hooning, M. J., *et al.* (2021) Estrogens and progestogens in triple negative breast cancer: do they harm? *Cancers (Basel)* **13**, 2506
66. Gueguinou, M., Chantome, A., Fromont, G., Bougnoux, P., Vandier, C., and Potier-Cartereau, M. (2014) KCa and Ca(2+) channels: the complex thought. *Biochim. Biophys. Acta.* **1843**, 2322–2333
67. Lee, N., Lim, B. H., Lee, K.-S., Shin, J., Pagire, H. S., Pagire, S. H., *et al.* (2021) Identification and characterization of a novel large-conductance calcium-activated potassium channel activator, CTIBD, and its relaxation effect on urinary bladder smooth muscle. *Mol. Pharmacol.* **99**, 114–124
68. Lee, N., Kim, S., Lee, N. Y., Jo, H., Jeong, P., Pagire, H. S., *et al.* (2024) Activation mechanism and novel binding sites of the $BK_{Ca}$ channel activator CTIBD. *Life Sci. Alliance* **7**, e202402621
69. Dick, G. M., Hunter, A. C., and Sanders, K. M. (2002) Ethylbromide tamoxifen, a membrane-impermeant antiestrogen, activates smooth muscle calcium-activated large-conductance potassium channels from the extracellular side. *Mol. Pharmacol.* **61**, 1105–1113
70. Gross, D., Bischof, H., Maier, S., Sporbeck, K., Birkenfeld, A. L., Malli, R., *et al.* (2022) $IK_{Ca}$ channels control breast cancer metabolism including AMPK-driven autophagy. *Cell Death Dis.* **13**, 902
71. Ohara, A., Saeki, Y., Nishikawa, M., Yamamoto, Y., and Yamamoto, G. (2006) Single-channel recordings of TREK-1 K+ channels in periodontal ligament fibroblasts. *J. Dental Res.* **85**, 664–669
72. Matt, L., Kim, K., Hergarden, A. C., Patriarchi, T., Malik, Z. A., Park, D. K., *et al.* (2018) α-Actinin anchors PSD-95 at postsynaptic sites. *Neuron* **97**, 1094–1109.e1099
73. Pham, T., Hussein, T., Calis, D., Bischof, H., Skrabak, D., Cruz Santos, M., *et al.* (2023) BK channels sustain neuronal $Ca^{2+}$ oscillations to support hippocampal long-term potentiation and memory formation. *Cell. Mol. Life Sci.* **80**, 369
74. Santos, M. C., Birkenfeld, L., Pham, T., Maier, S., Paulus, K., Ullemeyer, L., *et al.* (2025) Angiotensin II-induced cardiac fibrosis and dysfunction are exacerbated by deletion of cGKI in periostin+ myofibroblasts. *Clin Sci (Lond)* **139**, 507–526
75. Madhavi Sastry, G., Adzhigirey, M., Day, T., Annabhimoju, R., and Sherman, W. (2013) Protein and ligand preparation: parameters, protocols, and influence on virtual screening enrichments. *J. Computer. Aided. Mol. Des.* **27**, 221–234
76. Lu, C., Wu, C., Ghoreishi, D., Chen, W., Wang, L., Damm, W., *et al.* (2021) OPLS4: improving force field accuracy on challenging regimes of chemical space. *J. Chem. Theor. Comput.* **17**, 4291–4300
77. Halgren, T. A. (2009) Identifying and characterizing binding sites and assessing druggability. *J. Chem. Inf. Model.* **49**, 377–389
78. Halgren, T. (2007) New method for fast and accurate binding-site identification and analysis. *Chem. Biol. Drug Des.* **69**, 146–148
79. Halgren, T. A., Murphy, R. B., Friesner, R. A., Beard, H. S., Frye, L. L., Pollard, W. T., *et al.* (2004) Glide: a new approach for rapid, accurate docking and scoring. 2. Enrichment factors in database screening. *J. Med. Chem.* **47**, 1750–1759

80. Farid, R., Day, T., Friesner, R. A., and Pearlstein, R. A. (2006) New insights about HERG blockade obtained from protein modeling, potential energy mapping, and docking studies. *Bioorg. Med. Chem.* **14**, 3160–3173
81. Friesner, R. A., Murphy, R. B., Repasky, M. P., Frye, L. L., Greenwood, J. R., Halgren, T. A., *et al.* (2006) Extra precision glide: docking and scoring incorporating a model of hydrophobic enclosure for protein–ligand complexes. *J. Med. Chem.* **49**, 6177–6196
82. Yan, J, and Aldrich, RW (2012) BK potassium channel modulation by leucine-rich repeat-containing proteins. *Proc Natl Acad Sci U S A* **109**, 7917–7922